Biogeosciences, 10, 8109–8128, 2013
www.biogeosciences.net/10/8109/2013/
doi:10.5194/bg-10-8109-2013


Biogeosciences Open Access

# Climate change impacts on sea–air fluxes of $CO_2$ in three Arctic seas: a sensitivity study using Earth observation

**P. E. Land[1], J. D. Shutler[1], R. D. Cowling[2], D. K. Woolf[2], P. Walker[1], H. S. Findlay[1], R. C. Upstill-Goddard[3], and C. J. Donlon[4]**

[1]Plymouth Marine Laboratory, Prospect Place, West Hoe, Plymouth PL1 3DH, UK
[2]International Centre for Island Technology, Heriot-Watt University, Stromness, Orkney, KW16 3AW, UK
[3]School of Marine Science and Technology, Ridley Building, Newcastle University, NE1 7RU, UK
[4]European Space Agency, ESTEC/EOP-SME, Keplerlaan 1, 2201 AZ, Noordwijk, the Netherlands

*Correspondence to:* P. E. Land (peland@pml.ac.uk)

Received: 26 July 2012 – Published in Biogeosciences Discuss.: 12 September 2012
Revised: 2 August 2013 – Accepted: 12 November 2013 – Published: 11 December 2013

**Abstract.** We applied coincident Earth observation data collected during 2008 and 2009 from multiple sensors (RA2, AATSR and MERIS, mounted on the European Space Agency satellite Envisat) to characterise environmental conditions and integrated sea–air fluxes of $CO_2$ in three Arctic seas (Greenland, Barents, Kara). We assessed net $CO_2$ sink sensitivity due to changes in temperature, salinity and sea ice duration arising from future climate scenarios. During the study period the Greenland and Barents seas were net sinks for atmospheric $CO_2$, with integrated sea–air fluxes of $-36 \pm 14$ and $-11 \pm 5$ Tg C yr$^{-1}$, respectively, and the Kara Sea was a weak net $CO_2$ source with an integrated sea–air flux of $+2.2 \pm 1.4$ Tg C yr$^{-1}$. The combined integrated $CO_2$ sea–air flux from all three was $-45 \pm 18$ Tg C yr$^{-1}$. In a sensitivity analysis we varied temperature, salinity and sea ice duration. Variations in temperature and salinity led to modification of the transfer velocity, solubility and partial pressure of $CO_2$ taking into account the resultant variations in alkalinity and dissolved organic carbon (DOC). Our results showed that warming had a strong positive effect on the annual integrated sea–air flux of $CO_2$ (i.e. reducing the sink), freshening had a strong negative effect and reduced sea ice duration had a small but measurable positive effect. In the climate change scenario examined, the effects of warming in just over a decade of climate change up to 2020 outweighed the combined effects of freshening and reduced sea ice duration. Collectively these effects gave an integrated sea–air flux change of +4.0 Tg C in the Greenland Sea, +6.0 Tg C in the Barents Sea and +1.7 Tg C in the Kara Sea, reducing the Greenland and Barents sinks by 11 % and 53 %, respectively, and increasing the weak Kara Sea source by 81 %. Overall, the regional integrated flux changed by +11.7 Tg C, which is a 26 % reduction in the regional sink. In terms of $CO_2$ sink strength, we conclude that the Barents Sea is the most susceptible of the three regions to the climate changes examined. Our results imply that the region will cease to be a net $CO_2$ sink in the 2050s.

## 1 Introduction

### 1.1 Motivation

The Arctic Ocean covers a relatively small area ($\sim 10.7 \times 10^6$ km$^2$) of the global ocean and $\sim 53$ % of Arctic waters are broad and shallow (< 200 m) continental shelves. Consequently, the Arctic Ocean contributes only $\sim 1$ % to the global ocean volume but it is nevertheless thought to account for 5–14 % of the total oceanic sink for anthropogenic $CO_2$ (Bates and Mathis, 2009), largely due to strong seasonal biological drawdown (Takahashi et al., 2009). Given this disproportionate contribution, its susceptibility to environmental changes that include rapid warming well above the global average (Polyakov et al., 2010; Purkey and Johnson, 2010), accelerating sea ice retreat (Kwok et al., 2009), increasing freshwater inputs (Dai et al., 2009) and changes to ecosystem structure and primary

Published by Copernicus Publications on behalf of the European Geosciences Union.

productivity (Arrigo et al., 2008; Pabi et al., 2008) afford the Arctic Ocean an important role in future ocean $CO_2$ uptake.

The high uncertainty in the size of the Arctic Ocean $CO_2$ sink reflects a paucity of coordinated in situ measurement campaigns and difficulties of logistical support in a remote and hostile environment, especially during winter ice cover (Bates and Mathis, 2009). Moreover, the heterogeneous nature of Arctic waters, especially on the continental shelves, will likely confound future efforts that may aim to improve this estimate by extrapolating from temporally and spatially limited in situ data alone.

A potential alternative solution lies in exploiting satellite Earth observation (EO) data, as previously used to derive sea–air fluxes of $CO_2$ at the global scale (e.g. Boutin et al., 2002). The improved quasi-global availability of EO data has facilitated recent studies of $CO_2$ sea–air exchange over a substantial area of the Arctic Ocean (Arrigo et al., 2010; Else et al., 2008).

In this paper we apply spatially and temporally co-incident EO data, obtained from the European Space Agency's (ESA) environmental monitoring satellite Envisat, to evaluate the sensitivity of air–sea $CO_2$ exchange in three Arctic seas (Greenland, Barents, Kara) to changes in temperature, salinity and sea ice duration arising from future climate scenarios. We also consider the likely impacts of surface ocean biology on $CO_2$ fluxes through suppression of the transfer velocity ($k$) of $CO_2$ and the degree to which the potential uptake of $CO_2$ may be offset by outgassing via remineralisation of river-borne dissolved organic carbon (DOC) on Arctic shelves.

### 1.2 Study area

This study focuses on three Arctic seas, the Greenland, Barents and Kara seas. The geographical extent of these seas is defined by International Hydrographic Organization (1953) and shown in Fig. 1.

The Greenland Sea provides the only deep (2600 m) connection from the Arctic Ocean to the Global Ocean (ACIA, 2005) (via the Atlantic) and thus provides a direct link between these deep ocean waters and adjoining coastal waters of the Barents Sea (Fig. 1). It is a major source of warm, saline Atlantic water to the Arctic Ocean through the Fram Strait. Cool, fresher water extends south from the Fram Strait along its western boundary (ACIA, 2005), along which sea ice accumulates during winter. The Greenland Sea has been estimated to be a $CO_2$ sink with average integrated sea–air $CO_2$ flux of $-38\,\mathrm{Tg\,C\,yr^{-1}}$ (Arrigo et al., 2010).

The Barents Sea, the largest of the Arctic Ocean marginal seas, is a broad and shallow (maximum depth $\sim 450$ m) "inflow" shelf sea (Bates and Mathis, 2009), i.e. it is characterised by nutrient-rich oceanic inflows that sustain high seasonal primary productivity, with the potential for strong $CO_2$ uptake from the atmosphere. Freshwater inputs are comparatively small. It is bounded to the south by Scandinavia and

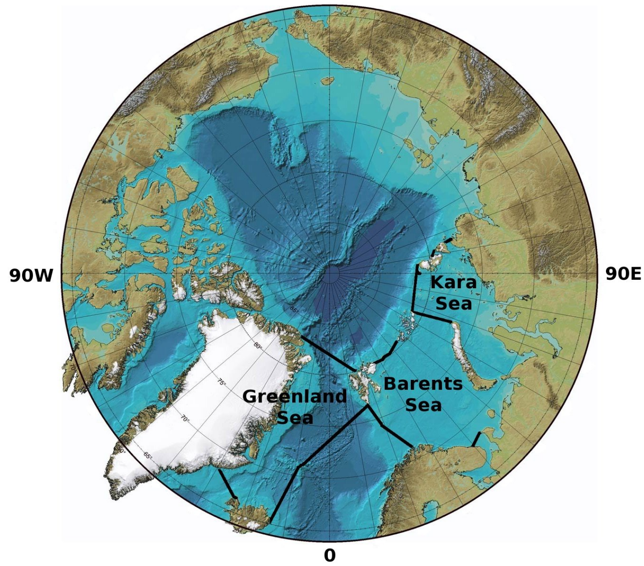


**Fig. 1.** The study area.

its eastward connection to the adjacent Kara Sea is restricted by the island of Novaya Zemlya (Fig. 1). An inflow of warm Atlantic surface water from the Norwegian Sea via the Norwegian Atlantic Current is characteristic of the Barents Sea during the summer months (Omar et al., 2007). Sea ice formation during subsequent cooling gives rise to densification and export to the Kara Sea and central Arctic Ocean basin as dense subsurface water (Fransson et al., 2001; Kaltin et al., 2002; Omar et al., 2007). The Barents Sea has been estimated to be a $CO_2$ sink with integrated sea–air $CO_2$ flux between $-24$ and $-77\,\mathrm{Tg\,C\,yr^{-1}}$ (Fransson et al., 2001; Kaltin et al., 2002; Nakaoka et al., 2006; Omar et al., 2007; Arrigo et al., 2010).

By contrast the Kara Sea is an "interior shelf" sea (Bates and Mathis, 2009), i.e. one which is highly influenced by exchanges with adjacent shelves. It receives inputs from the Barents Sea and exports water to the central Eurasian Basin. Due to the major inputs from the Ob and Yenisey rivers it is significantly less saline than the adjoining Barents Sea, with extremely low salinity waters extending some distance offshore. It also has a higher rate of sea ice production than other areas of the Arctic Ocean. Surface water $p\mathrm{CO_2}$ is spatially and temporally variable. Significant undersaturation has been observed following ice melt, whereas high supersaturation characterises coastal regions influenced by continental outflow (Bates and Mathis, 2009). The Kara Sea has been estimated to be a much smaller $CO_2$ sink than the Greenland or Barents seas, with integrated sea–air $CO_2$ flux between $-1$ and $-12\,\mathrm{Tg\,C\,yr^{-1}}$ (Anderson et al., 1998a, b; Fransson et al., 2001; Arrigo et al., 2010).

## 2 Methods

### 2.1 Data sets

We used EO data from the European Space Agency's (ESA) Environmental monitoring satellite, Envisat. Envisat was launched into a sun-synchronous near-polar orbit in 2002 and carried the Radar Altimeter 2 (RA2), the Advanced Along Track Scanning Radiometer (AATSR) and the Medium Resolution Imaging Spectrometer (MERIS). In the absence of clouds, AATSR and MERIS are capable of providing daily spatially and temporally coincident $T_{skin}$ and visible wavelength water reflectance over a broad swath. RA2 provides estimates of wind speed at 10 m height ($U_{10}$) and significant wave height ($H_S$) at the sub-satellite point. AATSR is a self-calibrating radiometer (Edwards et al., 1990) that provides estimates of surface skin temperatures (Donlon et al., 2007) and exhibits a very small standard deviation of error of 0.16 °C and a bias of +0.2 °C (O'Carroll et al., 2008). RA2 provides estimates of $U_{10}$ with a standard deviation of $1.25\,\mathrm{m\,s^{-1}}$ and a bias of $-0.28\,\mathrm{m\,s^{-1}}$, and $H_S$ with a standard deviation of 0.15 m and no global bias (Queffeulou et al., 2010). MERIS provides precision water reflectance at a number of visible wavelengths, which we use in combination with the AATSR data to estimate net primary production.

The level 2 RA2 altimeter data for 2008–2009 were preprocessed following ESA guidelines (Faugère et al., 2007) and were then extracted, quality filtered and binned to a $1^\circ \times 1^\circ$ geographic (equirectangular) grid using the ESA Basic Radar Altimetry Toolbox (BRAT) version 2.1.1 (Rosmorduc et al., 2009). Only valid ocean data were retained for analysis using the ESA-defined and orbit-specific ocean masking option within BRAT which implements the ESA recommendations. In addition, all $H_S$ data were corrected for known biases following the work of Queffeulou et al. (2010). The $1^\circ \times 1^\circ$ spatial grid was chosen as a compromise between the high spatial resolution data available from Envisat and the need to ensure completeness of the data coverage in space and time.

The level 2 AATSR two- and three-channel dual-view $T_{skin}$ data (referred to in the literature as D2 and D3 data, respectively) for 2008–2009 were extracted using the ESA Earth observation toolbox and development platform (BEAM) command line tools (BEAM, 2010). Following the AATSR masking procedures (Birks, 2007), data were only retained if (i) the nadir and dual $T_{skin}$ were valid (level 2 flags bits 0 and 2); (ii) the pixel was over the ocean (bit 4); and (iii) no cloud was present in either view (bits 5 and 8). The resultant level 2 data were binned to the same grid as the RA2 data using the BEAM binning tool.

The level 2 MERIS reduced resolution data for 2008–2009 were quality-filtered to remove cloud, land and negative reflectances using the ESA level 2 flags (bits 23, 22 and 20, respectively). These data were then re-projected to the same $1^\circ \times 1^\circ$ grid as the AATSR and RA2 data. Estimates of global primary productivity were then generated using coincident data from MERIS and AATSR and the primary productivity algorithm of Smyth et al. (2005). This primary productivity algorithm is based on a radiative transfer model, meaning that the approach is able to produce realistic estimates in both open-ocean (case I) and coastal (case II) waters. Its performance has been globally assessed (Smyth et al., 2005) and its use of a lookup table allows the efficient calculation of large data sets, such as the multi-year data used in this study. In both the AATSR and MERIS case, the single dominant error source is the full removal of cloud-contaminated data from the data set, which can be challenging in the presence of sea ice. We rely on the BEAM tools to perform cloud-flagging operations prior to gridding the data.

Climatological values including $p\mathrm{CO_{2W}}$ and salinity ($S$) were obtained from the Takahashi et al. (2009) climatology. Global daily air pressure and temperature fields were provided by the European Centre for Medium-range Weather Forecasting (ECMWF) operational data set (N80 Gaussian gridded analysis on surface levels; ERA-40 format, six-hourly fields). The Takahashi and ECMWF data were reprojected from their original 4° latitude by 5° longitude and $2.5^\circ \times 2.5^\circ$ grids, respectively, to the $1^\circ \times 1^\circ$ grid using bilinear interpolation (Kettle et al., 2009). Though the grid size was decreased, this was not an attempt to improve the resolution of the data sets, but simply to ensure that all data (climatology and EO) were on the same grid. No extrapolation beyond the bounds of the original data was performed, so this procedure should not introduce any bias or additional uncertainty. We note that use of, e.g. the Takahashi et al. (2009) data without this reprojection and interpolation, in conjunction with the $1^\circ \times 1^\circ$ EO data, would introduce discontinuities in the flux maps at the Takahashi et al. (2009) cell boundaries.

Daily values of the foundation temperature ($T_{fnd}$), defined as the temperature at a nominal depth of 0.2–1 m just before sunrise, were provided by the Operational Sea Surface Temperature and Sea Ice Analysis (OSTIA) system (Donlon et al., 2011; Stark et al., 2008), with a measured uncertainty of 0.6 °C and no significant global bias (Donlon et al., 2011). The sea ice analysis (within the OSTIA data) provides an estimate of the daily percentage sea ice coverage provided by the EUMETSAT Ocean and Sea Ice Satellite Application Facility (OSI-SAF) daily analyses. These daily global OSTIA $T_{fnd}$ and sea ice coverage data were averaged from their original $0.05^\circ \times 0.05^\circ$ grid to the same $1^\circ \times 1^\circ$ grid. For determining the characteristics within the three oceanic regions, the International Hydrographic Organization (IHO) boundaries of the major seas and oceans were obtained in a shape file (VLIZ) and then projected to a $0.1^\circ \times 0.1^\circ$ subgrid. For each cell of the $1^\circ \times 1^\circ$ grid (consisting of 100 subgrid cells classified as either within or outside the sea boundary), the proportion of subgrid cells that lie within a given sea boundary was recorded. This was 1 or 0 for most cells and intermediate on boundary cells. The use of a higher spatial resolution grid for the sea boundaries gives a more accurate representation of the spatial extent of each sea than using a mask at 1° resolution.

### 2.2 Calculating sea–air $CO_2$ fluxes

We estimated the sea-to-air flux of $CO_2$ ($F$, in $\mathrm{g\,m^{-2}\,s^{-1}}$) as the product of a gas transfer velocity, $k$ ($\mathrm{m\,s^{-1}}$), and the difference in $CO_2$ concentration ($\mathrm{g\,m^{-3}}$) between the base [$CO_{2AQW}$] and the top [$CO_{2AQ0}$] of a thin (∼ 250 µm) mass boundary layer at the sea surface:

$$F = k\left(\left[CO_{2AQW}\right] - \left[CO_{2AQ0}\right]\right). \tag{1}$$

The concentration of $CO_2$ in seawater is the product of its solubility, $\alpha$ ($\mathrm{g\,m^{-3}\,\mu atm^{-1}}$), and its fugacity, $fCO_2$ (µatm). As gas solubility is a function of salinity and temperature, it varies across the aqueous boundary layer. Hence Eq. (1) now becomes

$$F = k\left(\alpha_W fCO_{2W} - \alpha_S fCO_{2A}\right), \tag{2}$$

where the subscripts denote values in water (W), at the sea–air interface (S) (here assumed to be the sea skin) and in air (A). In practice however, sea surface $CO_2$ concentration is typically measured a few metres below the sea surface rather than at the bottom of the mass boundary layer. For simplicity we substitute partial pressure for fugacity because their values differ by $< 0.5\,\%$ over the temperature range considered (McGillis and Wanninkhof, 2006). Equation (2) can therefore be alternatively represented as

$$F = k\left(\alpha_W pCO_{2W} - \alpha_S pCO_{2A}\right). \tag{3}$$

Various authors have parameterized $k$ in terms of wind speed or sea state. In this work we chose to analyse our results using two empirical parameterizations using the wind speed (Nightingale et al., 2000; Ho et al., 2006) and a physically based parameterization (Fangohr and Woolf, 2007).

We used the data sets and methodology described below to produce daily maps of $F$, which we then used to estimate the integrated $CO_2$ flux for the Greenland, Barents and Kara seas. We then investigated the sensitivity of these values to changes in the input parameters.

#### 2.2.1 Partial pressure of $CO_2$

Takahashi et al. (2009) provide climatological estimates of $F$ and the variables required for its derivation, along with a method for correcting the climatology to any given year. These data were generated from over three million in situ measurements of surface water $pCO_2$ obtained between 1970 and 2007, though time-space coverage of the Arctic in the Takahashi data is highly limited (Takahashi et al., 2009). The Takahashi data are referenced to a standard non-El-Niño year (2000), so associated measurement-uncertainties for the $CO_2$ fluxes in other years are likely to be larger. To reduce these uncertainties and to correct for the increase in global $CO_2$ since 2000, these climatology data were modified to the prevailing physical conditions in 2008–2009.

$pCO_{2W}$ (referenced to year 2000 in the Takahashi climatology) was corrected to the temperature and salinity conditions for the period of study and increased by $1.5\,\mathrm{\mu atm\,yr^{-1}}$ (Takahashi et al., 2009; Kettle et al., 2009) using

$$\begin{aligned} pCO_{2W} = pCO_{2W}^{Tak} \exp\Big[&0.0423\left(SST_{fnd} - T^{Tak}\right) \\ &-4.35\times10^{-5}\left\{(SST_{fnd})^2 - \left(T^{Tak}\right)^2\right\} \\ &+1.7\left(S - S^{Tak}\right)/S^{Tak}\Big] + 1.5\,(\text{year} - 2000). \end{aligned} \tag{4}$$

The temperature adjustment (the first two terms in the exponential) is given by Takahashi et al. (2009). The salinity adjustment (the third term in the exponential) is from Sarmiento and Gruber (2006):

$$\frac{\partial pCO_2}{\partial S} = \gamma_S \frac{pCO_2}{S}, \tag{5}$$

where $\gamma_S$ has a value of about 1 when comparing waters of the same dissolved inorganic carbon (DIC) content, e.g. two oceanic water masses with the same DIC and temperature but with different salinities. However, when considering the effect of freshening due to waters with negligible DIC (e.g. rainwater), the value increases to 1.6 at low latitudes and 1.7 at high latitudes. Rysgaard et al. (2007) present evidence that 75 % or more of DIC is rejected together with brine from growing sea ice, hence we used $\gamma_S = 1.7$ in Eq. (4). This is valid in seas where the major contribution to climate-related freshening is due to ice melt, but is inappropriate if the major contribution comes from increased DIC-laden river runoff, which could be the case in the Kara Sea.

Temporal averaging of sea-level air pressure has been shown by Kettle and Merchant (2005) to introduce large errors in flux calculations. Therefore $pCO_{2A}$ (in µatm) was determined from the atmospheric climatology data and increased by $1.5\,\mathrm{\mu atm\,yr^{-1}}$ using:

$$pCO_{2A} = 0.001 X_{[CO]_2}^{Tak}\left(P - pH_2O\right) + 1.5\,(\text{year} - 2000) \tag{6}$$

where $X_{[CO]_2}^{Tak}$ is the mole fraction of $CO_2$ in the dry atmosphere from the Takahashi climatology in parts per million, $P$ is the daily average air pressure in mbar from the ECMWF data, 1013.25 is standard atmospheric pressure and $pH_2O$ is the saturation vapour pressure of water in mbar, which is defined by Weiss and Price (1980) in terms of temperature $T_K$ (Kelvin) and salinity $S$ (PSU) as

$$\begin{aligned} pH_2O = 1013.25\exp\Big(&24.4543 - 67.4509\frac{100}{T_K} \\ &- 4.8489\ln\frac{T_K}{100} - 0.000544S\Big), \end{aligned} \tag{7}$$

where $T_K = T_{skin} + 273.15$.

### 2.2.2 Gas transfer velocity

Daily maps of the gas transfer velocity $k$ (in $\mathrm{m\,s^{-1}}$) were derived from the $1° \times 1°$ AATSR and RA2 data using three different approaches. We investigated two different empirical wind-based gas transfer velocity parameterizations and one based on the physics of the sea surface, to provide an indication of the potential errors introduced by different gas transfer parameterizations in the three Arctic seas.

The first parameterization (Nightingale et al., 2000) is based on $U_{10}$ and $T_{\mathrm{skin}}$ and uses an empirical relationship derived from field data predominantly obtained in shelf seas:

$$k = \left(0.333U_{10} + 0.222U_{10}^2\right)(Sc/600)^{-0.5}, \tag{8}$$

where $Sc$ is the Schmidt number given by Wanninkhof (1992) as

$$Sc = 2073.1 - 125.62T_{\mathrm{skin}} + 3.6276\,(T_{\mathrm{skin}})^2 - 0.043219\,(T_{\mathrm{skin}})^3. \tag{9}$$

The second parameterization (Ho et al., 2006) uses data from the Southern Ocean to produce a similar relationship:

$$k = 0.266U_{10}^2\,(Sc/600)^{-0.5}. \tag{10}$$

This was shown by Ho et al. (2011) to have global applicability.

The third parameterization (Fangohr and Woolf, 2007) is physically based and is derived from field and model data. It uses a combination of $U_{10}$, $H_{\mathrm{S}}$, the backscatter coefficient $\sigma_0$ and $T_{\mathrm{skin}}$. This approach uses the hybrid model of Woolf (2005) to determine $k$, defined as $k = k_{\mathrm{d}} + k_{\mathrm{b}}$, where $k_{\mathrm{d}}$ is the direct gas transfer and $k_{\mathrm{b}}$ is the bubble-mediated transfer. Bubble-mediated transfer is the enhancement of sea–air gas transfer resulting from oceanic wave breaking, or whitecapping (Woolf et al., 2007). This aspect of gas transfer is not explicitly characterized in the wind parameterizations of Nightingale et al. (2000) or Ho et al. (2006). Please refer to Fangohr and Woolf (2007) and Goddijn-Murphy et al. (2012) for a detailed description of this approach.

### 2.2.3 Solubility

The solubility $\alpha$ of $CO_2$ in sea water is a function of $T_{\mathrm{K}}$ and $S$ given by Weiss (1974) as

$$\alpha = 0.012\exp\left[A + B\frac{100}{T_{\mathrm{K}}} + C\ln\left(\frac{T_{\mathrm{K}}}{100}\right) + S\left\{D + E\frac{T_{\mathrm{K}}}{100} + G\left(\frac{T_{\mathrm{K}}}{100}\right)^2\right\}\right], \tag{11}$$

where $T_{\mathrm{K}} = T_{\mathrm{fnd}} + 273.15$ in the case of $\alpha_{\mathrm{W}}$ and $T_{\mathrm{K}} = T_{\mathrm{skin}} + 273.15$ in the case of $\alpha_{\mathrm{S}}$, $A = -60.2409$, $B = 93.4517$, $C = 23.3585$, $D = 0.023517$, $E = -0.023656$ and $G = 0.0047036$.

### 2.2.4 Integrated $CO_2$ fluxes

Together, Eqs. (3)–(11) allow calculation of $F$ per unit area of open water. Sea ice coverage data were used with $F$ to calculate the integrated $CO_2$ flux from a 1° by 1° grid cell (Takahashi et al., 2009). A clear distinction should be made in the following between $F$, which is the flux per unit area and time at a given point, and integrated flux, which is the sum of (positive and/or negative) flux through a given area, be it a grid cell or a geographical region such as a sea, over a given time, e.g. a month or a year. In the case of a grid cell containing ice or land, we use the open water value of $F$, and modify the calculation of integrated flux to account for the ice or land cover.

Following Takahashi et al. (2009), we considered sea ice coverage $< 10\,\%$ to have a negligible effect on the integrated $CO_2$ flux from a cell, so in this case sea ice coverage was set to zero, whereas sea ice coverage $> 90\,\%$ still allows some flux of $CO_2$ due to leads, polynyas etc. (where air–sea heat fluxes may be very strong), so in this case ice coverage was set to 90 %. Multiplying $F$ (per unit area) by the remaining ice free surface area gives the integrated $CO_2$ flux from the cell.

Fluxes in marginal ice zones may be enhanced over a simple proportionality to ice-free area (Loose et al., 2009; Else et al., 2011). We use the parameterization suggested by Loose et al. (2009), that flux is proportional to (ice-free proportion)$^{0.4}$. We do this by modifying the ice coverage to give an 'effective ice-free area' in each cell, while continuing to use the open water estimate of $F$. For instance, cells with ice coverage $\geq 90\,\%$ will have an effective ice-free area of 40 % of the cell area, reducing the integrated cell flux to 40 % of the open water value.

$F$ was only calculated in cells where all the required data were available. In a given sea, the total effective ice-free area $A_{\mathrm{miss}}$ of cells with no flux data was also calculated, as was the mean flux $\bar{F}$ due to all cells in the sea with flux data. The product $A_{\mathrm{miss}}\bar{F}$ was then added to the integrated flux due to cells with flux data, to give an estimate of the integrated $CO_2$ flux across the sea surface. This procedure enables a first-order correction for the flux in regions where there are no EO data. Its use assumes that the mean $F$ within the missing region is the same as the mean $F$ within the regions where EO data are present. In cases where no values of $F$ could be calculated for a given sea (this occurred for the Kara Sea in March to May), the monthly $\bar{F}$ was linearly interpolated between the nearest valid months.

## 2.3 Sensitivity to salinity, temperature and sea ice duration

The Arctic Ocean is considered very susceptible to the impacts of a changing climate, with a large range of conditions predicted by 2020 (ACIA, 2005). Although the Arctic has changed greatly since the publication of ACIA (2005), the more recent IPCC Fourth Assessment Report (Denman et al., 2007) is insufficiently detailed to allow predictions of changes for the three seas studied here. We therefore consider the predictions of ACIA (2005) to represent a plausible range of climate change effects, providing a framework within which to examine sensitivity. Following the changes in Arctic climate predicted by ACIA (2005), we performed an analysis to investigate the sensitivity of the integrated sea–air fluxes of $CO_2$ to increased temperature, reduced salinity (freshening) and decreased sea ice duration. The impact of changes in each of these quantities was considered individually, and we also estimated the combined effects of the 2020 scenario predicted by ACIA (2005).

Over the 20 yr from a baseline ending in 2000 to 2020, ACIA (2005) predict an Arctic-wide increase in annual mean sea surface temperature of 1 to 1.5 °C, further divided into 2.5 °C in winter and 0.5 °C in summer, and a salinity reduction of 0.1 to 0.3 PSU in the southeast Barents Sea and the Kara Sea with a weak (unspecified) freshening along the East Greenland coast. The predicted effects on sea ice are an Arctic-wide reduction in sea ice duration of 10 days and a 6–10 % reduction in winter extent, with the shelf seas likely to be ice-free in summer. Clearly the above information is insufficiently detailed to make a definitive 2020 $CO_2$ integrated flux prediction in each sea, but here we give an impression of the effects of plausible changes in temperature, salinity and sea ice duration from 2008–2009 to 2020 by taking the average of the above ranges of variation in the change from year 2000 to year 2020 and scaling linearly to a change from years 2008–2009 to year 2020, i.e. multiplying by $(2020 - 2008.5) / (2020 - 2000) = 0.575$. This gives a warming of 0.7 °C, a freshening of 0.1 PSU and a reduction in sea ice duration of 6 days, each of which is assumed to apply uniformly over all three seas. The Arctic-wide reduction in winter sea ice extent of 5 % and the prediction that the shelves are likely to be ice free in summer are difficult to implement in a specific location. Instead, we assume these to emerge as a result of the reduction in sea ice duration. The sensitivity of integrated $CO_2$ flux to each of the different parameters was investigated by varying one parameter while keeping the others fixed at their original values, applying parameter changes uniformly across all valid data. For the temperature sensitivity, $T_{\mathrm{fnd}}$ and $T_{\mathrm{skin}}$ were assumed to covary. Temperature variations were applied to all temperature-dependent components of Eq. (3) and its sub-equations ($\alpha_\mathrm{S}$, $\alpha_\mathrm{W}$, $k$, $p\mathrm{CO}_{2\mathrm{W}}$, $p\mathrm{H_2O}$). The salinities at the surface and at a depth of a few meters were also assumed to co-vary. Salinity variations were applied to all salinity-dependent components of Eq. (3) and its sub-equations ($\alpha_\mathrm{S}$, $\alpha_\mathrm{W}$, $p\mathrm{CO}_{2\mathrm{W}}$, $p\mathrm{H}_2O$).

To simulate changes in sea ice cover, on a given day (here labeled day 0) we calculated the reduction in integrated $CO_2$ flux from each cell due to sea ice several times, first using the sea ice on day 0, then on days −1 and 1, −2 and 2 etc. Depending on the season, the sea ice cover may be broadly increasing (autumn freezing), decreasing (spring thaw) or static (midsummer or midwinter). To simulate the effect of a general reduction/increase in sea ice duration of $2N$ days, we took the minimum/maximum sea ice amount in a time window from day $-N$ to day $N$, where $N$ was varied from 1 to 3. This had the effect of moving the spring thaw earlier/later and the autumn freeze later/earlier, both by $N$ days. The effects on winter and summer depend on the day to day variability of sea ice cover during these seasons. Figure 2 shows the effect of a two-day reduction/increase in sea ice duration ($N = 1$) in a fictitious example with 30 days per year.

These assumptions allow us to gain further insight into the impact of plausible changes in temperature, salinity and sea ice duration from 2008–2009 to 2020.

## 3 Results

### 3.1 Characterization of study area

Tables 1 to 5 and Fig. 3 show lower quartile, monthly median and upper quartile values of relevant properties of the three seas during 2008 and 2009, derived from our EO data. Areal ice coverage for each sea was calculated daily, and the monthly statistics were generated from all days in the month over both years. On each day, the remaining sea area was used to determine area-weighted histograms of the other EO derived quantities used in this paper: $T_{\mathrm{skin}}$ (°C), $U_{10}$ (m s$^{-1}$), $H_\mathrm{s}$ (m), and net primary production (PP) (mg C m$^{-2}$ day$^{-1}$). $H_\mathrm{s}$ is not shown in Fig. 3 as its variation (listed in Table 4) showed similar patterns to that of $U_{10}$. Figure 4 shows monthly mean sea ice coverage over the whole region during 2008 and 2009 combined, revealing the spatial and seasonal variations within each sea.

Figure 3a shows Greenland Sea ice cover to be dominated by the West Ice, which covers up to 37 % of its area in winter, retreating northwards to about 11 % in August and September. The Barents Sea was the least affected by sea ice, with a peak ice cover of 34 % in April, mostly in the north, retreating northwards to become negligible from July to October. The Kara Sea was the most affected by sea ice for most of the year, with a peak ice cover of about 90 % from February to May, retreating northwards to become negligible from August to October. Figure 3b shows the Barents Sea to be generally the warmest of the three seas, except from May to August, when it has similar temperatures to the Greenland Sea. The Kara Sea is the coolest except in August. From Fig. 3c and Table 4, the wind and wave climates are similar in the Greenland and Barents seas, whereas both wind and waves are lower in the Kara Sea, especially during the first half of the year. From Fig. 3d, PP follows a similar pattern in all three seas, and appears to follow light availability. However, the upper quartile PP (likely to represent algal blooms) in the Kara Sea is by far the greatest, suggesting that this sea is much more susceptible to summertime phytoplankton blooms. PP peaks in May in the Barents Sea, June

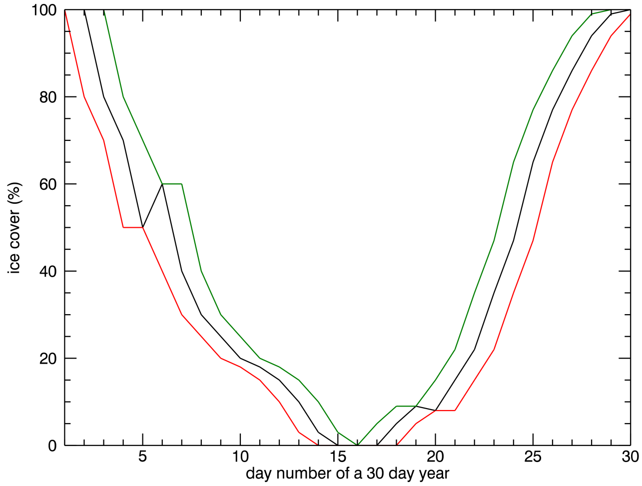


**Fig. 2.** Effect of a two-day reduction (red) or increase (green) in the sea ice duration in a fictional 30-day year. The black line shows the original values.

in the Greenland Sea and July in the Kara Sea. It should be noted that the PP value quoted is the production per unit clear (ice-free) sea area, not the total production over the sea.

### 3.2 Integrated $CO_2$ flux for each sea and differences between $k$ parameterizations

The mean daily clear water $CO_2$ flux $F$ over both years is shown in Fig. 5 using the Nightingale et al. (2000) $k$ parameterization (the flux using the Ho et al. (2006) $k$ parameterization is very similar), and the annual sea-integrated $CO_2$ fluxes using the two parameterizations are listed in Table 6. These show clearly that in 2008 and 2009 the Greenland Sea was a strong net sink of $CO_2$ (negative flux values) and the Barents Sea was a weaker sink, while the Kara Sea was a weak net source of $CO_2$. Also shown is the integrated $CO_2$ flux from all three seas grouped together. Fangohr and Woolf (2007) (not shown) give fluxes of the same sign as Nightingale et al. (2000) and Ho et al. (2006) but with about 1.75 times the magnitude, indicating a likely problem with the Fangohr and Woolf (2007) algorithm (see Sect. 4.4). Figure 6 shows the monthly mean $F$ over both years using the Nightingale et al. (2000) $k$ parameterization, showing clearly the seasonality of $F$ in the Greenland and Kara seas and the differing ice cover in the three seas. Figure 7 shows the monthly mean integrated $CO_2$ flux in each sea using Nightingale et al. (2000). Note that no $F$ value could be calculated in the Kara Sea from March to May for either year. These values were estimated by linearly interpolating from the adjacent months (shown by a dashed line).

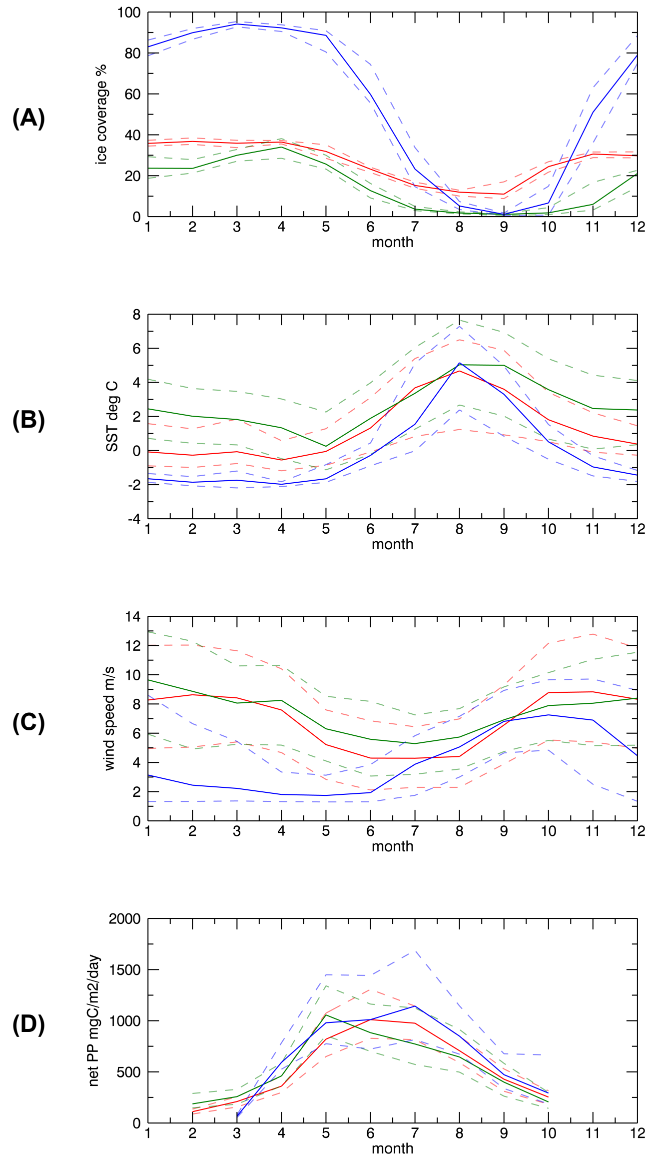


**Fig. 3.** Parameters retrieved from remote sensing: **(A)** sea ice coverage in %; **(B)** $T_{skin}$ in °C; **(C)** wind speed in $m\,s^{-1}$; **(D)** net primary production in $mg\,C\,m^{-2}\,day^{-1}$. Red lines indicate the Greenland Sea, green the Barents Sea and blue the Kara Sea. Solid lines show the median of all valid remotely sensed data, dashed lines show the lower and upper quartiles.

### 3.3 Effects of increased temperature, freshening and reduction in sea ice duration

The results of the different sensitivity studies using the Nightingale et al. (2000) $k$ parameterization are summarised in Table 7 and shown in Figs. 8 to 11. Results from the Ho et al. (2006) and Fangohr and Woolf (2007) $k$ parameterizations show similar sensitivities (not shown). The effect of increasing both $T_{fnd}$ and $T_{skin}$ uniformly over the whole region on the annual mean integrated $CO_2$ flux from each sea in each

**Table 1.** Lower quartile (Q1), median and upper quartile (Q3) monthly values of ice coverage (%) in the three seas.

| Month | Greenland Sea | | | Barents Sea | | | Kara Sea | | |
|---|---|---|---|---|---|---|---|---|---|
| | Q1 | median | Q3 | Q1 | median | Q3 | Q1 | median | Q3 |
| 1 | 35 | 36 | 37 | 19 | 24 | 29 | 79 | 83 | 86 |
| 2 | 35 | 37 | 38 | 21 | 24 | 28 | 87 | 90 | 92 |
| 3 | 34 | 36 | 37 | 27 | 30 | 33 | 93 | 94 | 95 |
| 4 | 36 | 36 | 37 | 29 | 34 | 38 | 91 | 92 | 94 |
| 5 | 29 | 32 | 35 | 23 | 26 | 30 | 81 | 89 | 91 |
| 6 | 22 | 23 | 24 | 9 | 13 | 16 | 56 | 60 | 74 |
| 7 | 14 | 15 | 17 | 3 | 4 | 5 | 15 | 23 | 34 |
| 8 | 10 | 12 | 13 | 1 | 2 | 2 | 3 | 5 | 7 |
| 9 | 9 | 11 | 17 | 1 | 1 | 2 | 1 | 1 | 2 |
| 10 | 22 | 24 | 27 | 1 | 2 | 4 | 1 | 7 | 15 |
| 11 | 29 | 31 | 32 | 3 | 6 | 17 | 36 | 51 | 63 |
| 12 | 29 | 30 | 32 | 15 | 21 | 23 | 75 | 79 | 89 |

**Table 2.** Lower quartile (Q1), median and upper quartile (Q3) monthly values of sea surface skin temperature $T_{skin}$ (°C) in the three seas.

| Month | Greenland Sea | | | Barents Sea | | | Kara Sea | | |
|---|---|---|---|---|---|---|---|---|---|
| | Q1 | median | Q3 | Q1 | median | Q3 | Q1 | median | Q3 |
| 1 | −0.9 | −0.1 | 1.6 | 0.7 | 2.4 | 4.2 | −1.9 | −1.7 | −1.3 |
| 2 | −1.0 | −0.3 | 1.3 | 0.4 | 2.0 | 3.6 | −2.1 | −1.9 | −1.5 |
| 3 | −0.8 | −0.1 | 1.8 | 0.3 | 1.8 | 3.5 | −2.2 | −1.7 | −1.2 |
| 4 | −1.2 | −0.6 | 0.6 | −0.5 | 1.3 | 3.0 | −2.1 | −2.0 | −1.8 |
| 5 | −0.9 | −0.1 | 1.3 | −1.1 | 0.3 | 2.3 | −1.9 | −1.7 | −0.8 |
| 6 | −0.1 | 1.3 | 3.1 | −0.2 | 1.9 | 4.0 | −0.9 | −0.3 | 0.4 |
| 7 | 0.8 | 3.7 | 5.4 | 1.3 | 3.4 | 6.0 | 0.0 | 1.5 | 5.1 |
| 8 | 1.2 | 4.7 | 6.5 | 2.7 | 5.0 | 7.7 | 2.4 | 5.2 | 7.3 |
| 9 | 0.9 | 3.6 | 5.9 | 2.0 | 5.0 | 6.9 | 0.8 | 3.3 | 5.0 |
| 10 | 0.5 | 1.8 | 3.4 | 0.7 | 3.6 | 5.4 | −0.5 | 0.5 | 1.5 |
| 11 | −0.1 | 0.8 | 2.2 | 0.1 | 2.5 | 4.4 | −1.5 | −1.0 | −0.3 |
| 12 | −0.3 | 0.4 | 1.5 | 0.3 | 2.4 | 4.1 | −1.8 | −1.4 | −1.2 |

**Table 3.** Lower quartile (Q1), median and upper quartile (Q3) monthly values of wind speed at 10 m $U_{10}$ (m $s^{-1}$) in the three seas.

| Month | Greenland Sea | | | Barents Sea | | | Kara Sea | | |
|---|---|---|---|---|---|---|---|---|---|
| | Q1 | median | Q3 | Q1 | median | Q3 | Q1 | median | Q3 |
| 1 | 5.0 | 8.3 | 12.0 | 5.9 | 9.6 | 12.9 | 1.3 | 3.1 | 8.6 |
| 2 | 5.1 | 8.6 | 12.0 | 4.9 | 8.9 | 12.3 | 1.3 | 2.4 | 6.7 |
| 3 | 5.4 | 8.4 | 11.6 | 5.2 | 8.1 | 10.6 | 1.4 | 2.2 | 5.4 |
| 4 | 4.7 | 7.6 | 10.4 | 5.2 | 8.2 | 10.6 | 1.3 | 1.8 | 3.3 |
| 5 | 2.8 | 5.2 | 7.6 | 4.1 | 6.3 | 8.5 | 1.3 | 1.7 | 3.1 |
| 6 | 2.1 | 4.3 | 6.9 | 3.1 | 5.6 | 8.2 | 1.3 | 1.9 | 3.9 |
| 7 | 2.3 | 4.3 | 6.4 | 3.2 | 5.3 | 7.3 | 1.7 | 3.9 | 5.8 |
| 8 | 2.3 | 4.4 | 7.0 | 3.5 | 5.7 | 7.7 | 3.0 | 5.1 | 7.2 |
| 9 | 3.9 | 6.6 | 9.3 | 4.7 | 6.9 | 9.2 | 4.7 | 6.8 | 8.9 |
| 10 | 5.5 | 8.8 | 12.2 | 5.5 | 7.9 | 10.1 | 4.8 | 7.3 | 9.7 |
| 11 | 5.4 | 8.8 | 12.8 | 5.2 | 8.1 | 11.1 | 2.5 | 6.9 | 9.7 |
| 12 | 5.0 | 8.3 | 11.8 | 5.2 | 8.4 | 11.5 | 1.3 | 4.5 | 8.9 |

**Table 4.** Lower quartile (Q1), median and upper quartile (Q3) monthly values of significant wave height $H_s$ (m) in the three seas.

| Month | Greenland Sea | | | Barents Sea | | | Kara Sea | | |
|---|---|---|---|---|---|---|---|---|---|
| | Q1 | median | Q3 | Q1 | median | Q3 | Q1 | median | Q3 |
| 1 | 0.6 | 0.8 | 1.2 | 0.6 | 0.9 | 1.2 | 0.1 | 0.5 | 0.7 |
| 2 | 0.5 | 0.8 | 1.1 | 0.6 | 0.8 | 1.1 | 0.0 | 0.3 | 0.5 |
| 3 | 0.5 | 0.7 | 0.9 | 0.5 | 0.6 | 0.8 | 0.0 | 0.0 | 0.3 |
| 4 | 0.4 | 0.6 | 0.8 | 0.4 | 0.6 | 0.8 | 0.0 | 0.0 | 0.3 |
| 5 | 0.3 | 0.4 | 0.6 | 0.3 | 0.4 | 0.6 | 0.0 | 0.1 | 0.3 |
| 6 | 0.3 | 0.4 | 0.5 | 0.3 | 0.4 | 0.6 | 0.0 | 0.2 | 0.3 |
| 7 | 0.3 | 0.4 | 0.5 | 0.3 | 0.4 | 0.5 | 0.2 | 0.3 | 0.4 |
| 8 | 0.3 | 0.4 | 0.6 | 0.3 | 0.4 | 0.5 | 0.2 | 0.3 | 0.4 |
| 9 | 0.4 | 0.6 | 0.8 | 0.4 | 0.6 | 0.8 | 0.3 | 0.5 | 0.6 |
| 10 | 0.5 | 0.8 | 1.1 | 0.5 | 0.6 | 0.9 | 0.4 | 0.5 | 0.7 |
| 11 | 0.5 | 0.8 | 1.2 | 0.5 | 0.7 | 1.0 | 0.3 | 0.5 | 0.7 |
| 12 | 0.6 | 0.8 | 1.1 | 0.5 | 0.8 | 1.0 | 0.2 | 0.4 | 0.6 |

**Table 5.** Lower quartile (Q1), median and upper quartile (Q3) monthly values of net primary production PP (mg C $m^{-2}$ $day^{-1}$) in the three seas.

| Month | Greenland Sea | | | Barents Sea | | | Kara Sea | | |
|---|---|---|---|---|---|---|---|---|---|
| | Q1 | median | Q3 | Q1 | median | Q3 | Q1 | median | Q3 |
| 1 | – | – | – | – | – | – | – | – | – |
| 2 | 88 | 111 | 136 | 148 | 187 | 289 | – | – | – |
| 3 | 157 | 210 | 257 | 184 | 258 | 329 | 53 | 66 | 80 |
| 4 | 298 | 360 | 458 | 362 | 460 | 585 | 526 | 593 | 784 |
| 5 | 650 | 820 | 1074 | 854 | 1056 | 1341 | 775 | 980 | 1449 |
| 6 | 828 | 1011 | 1307 | 700 | 883 | 1163 | 723 | 1011 | 1442 |
| 7 | 815 | 976 | 1143 | 572 | 772 | 1124 | 815 | 1143 | 1687 |
| 8 | 591 | 707 | 848 | 498 | 645 | 914 | 673 | 850 | 1145 |
| 9 | 311 | 428 | 529 | 263 | 400 | 583 | 338 | 472 | 677 |
| 10 | 184 | 253 | 315 | 144 | 206 | 299 | 187 | 293 | 665 |
| 11 | – | – | – | – | – | – | – | – | – |
| 12 | – | – | – | – | – | – | – | – | – |

year using the Nightingale et al. (2000) $k$ parameterization is shown in Fig. 8, with the 2020 prediction of 0.7 °C shown as a dotted line. The effect is a strongly linear ($r^2 > 0.999$) positive change in integrated flux, making the Greenland and Barents seas less absorbing and the Kara Sea more emitting. The mean integrated $CO_2$ flux changes per degree warming are: Greenland Sea +7.8 Tg C $°C^{-1}$ (−21 % $°C^{1}$); Barents Sea +11.1 Tg C $°C^{-1}$ (−99 % $°C^{-1}$); Kara Sea +3.2 Tg C $°C^{-1}$ (+149 % $°C^{-1}$). The combined effect on all three seas grouped together is +22.1 Tg C $°C^{-1}$ (−49 % $°C^{-1}$). The 2020 warming prediction of 0.7 °C causes integrated $CO_2$ flux changes (from 2008–2009 to 2020) of: Greenland Sea +5.0 Tg C (−14 %); Barents Sea +7.3 Tg C (−65 %); Kara Sea +2.1 Tg C (+99 %). The combined effect on all three seas grouped together is +14.5 Tg C $°C^{-1}$ (−29 %, i.e. a 29 % reduction in the regional sink).

The effect of decreasing salinity uniformly over the whole region on the annual mean integrated $CO_2$ flux from each sea in each year using the Nightingale et al. (2000) $k$ parameterization is shown in Fig. 9, with the 2020 prediction of 0.1 PSU shown as a dotted line. The effect is a strongly linear ($r^2 > 0.9999$) negative change in integrated flux with decreasing salinity, making the Greenland and Barents seas more absorbing and the Kara Sea less emitting. The mean integrated flux changes per PSU freshening are: Greenland Sea −8.6 Tg C $PSU^{-1}$ (+24 % $PSU^{-1}$); Barents Sea −12.4 Tg C $PSU^{-1}$ (+110 % $PSU^{-1}$); Kara Sea −4.0 Tg C $PSU^{-1}$ (−190 % $PSU^{-1}$). The combined effect on all three seas grouped together is −25.0 Tg C $PSU^{-1}$ (+55 % $PSU^{-1}$). The 2020 freshening prediction of 0.1 PSU (from 2008–2009 to 2020) causes integrated flux changes of: Greenland Sea −0.87 Tg C (+2.4 %); Barents Sea −1.24 Tg C (+11 %); Kara Sea −0.41 Tg C (−19 %). The combined effect on all three seas grouped together is −2.52 Tg C (+5.5 %).

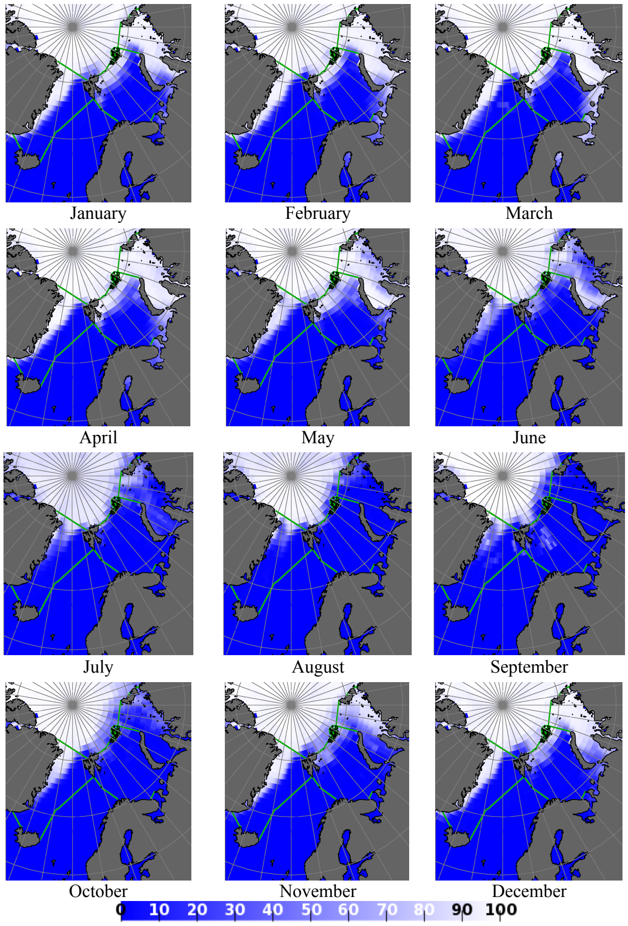


**Fig. 4.** Monthly mean sea ice coverage over the study region during 2008 and 2009 combined. White is ice, blue is ice-free, grey is land. Range is 0 to 100 % sea ice cover.

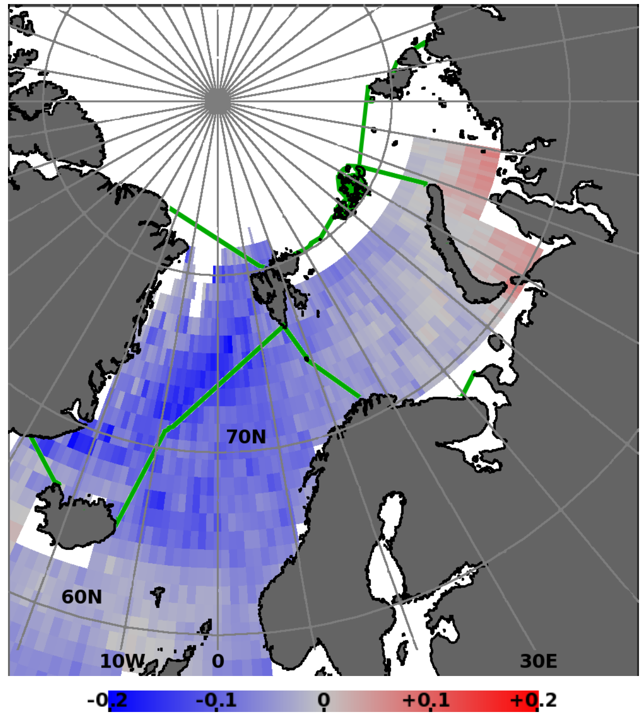


**Fig. 5.** Mean sea–air flux $F$ of $CO_2$ in $\mathrm{g\,C\,m^{-2}\,day^{-1}}$ during 2008 and 2009 combined using the $k$ parameterization of Nightingale et al. (2000). Blue is absorbing, red is emitting, dark grey is land, white is no data.

The effect of reducing the duration of sea ice cover uniformly over the whole region on the annual mean integrated $CO_2$ flux from each sea in each year using the Nightingale et al. (2000) $k$ parameterization is shown in Fig. 10, with the 2020 prediction of a 6-day reduction shown as a dotted line. The effect is a small and moderately linear ($r^2 > 0.92$) negative change in integrated flux, making the Greenland and Barents seas slightly more absorbing and the Kara Sea slightly less emitting. The mean integrated flux changes per day of duration reduction are: Greenland Sea $-0.030\,\mathrm{Tg\,C\,day^{-1}}$ (+0.08 % $\mathrm{day^{-1}}$); Barents Sea $-0.013\,\mathrm{Tg\,C\,day^{-1}}$ (+0.11 % $\mathrm{day^{-1}}$); Kara Sea $-0.00028\,\mathrm{Tg\,C\,day^{-1}}$ ($-0.01$ % $\mathrm{day^{-1}}$). The combined effect on all three seas grouped together is $-0.043\,\mathrm{Tg\,C\,day^{-1}}$ (+0.09 % $\mathrm{day^{-1}}$). The 2020 sea ice duration prediction of a 6-day reduction (from 2008–2009 to 2020) causes changes in annual integrated flux of: Greenland Sea $-0.20$ Tg C (+0.6 %); Barents Sea $-0.11$ Tg C (+1.0 %); Kara Sea $-0.022$ Tg C ($-1.0$ %). The combined effect on all three seas grouped together is $-0.33$ Tg C (+0.7 %).

The combined effect of all three of the predicted changes for 2020 (0.7 °C temperature increase, 0.1 PSU freshening, 6-day reduction in sea ice duration) using the Nightingale et al. (2000) $k$ parameterization is shown in Fig. 11. The positive change in integrated flux due to warming outweighs the negative changes due to salinity and sea ice duration so the net effect is a positive change in annual sea–air integrated $CO_2$ flux (from 2008–2009 to 2020) in all three seas: Greenland Sea +4.0 Tg C ($-11$ %); Barents Sea +6.0 Tg C ($-53$ %); Kara Sea +1.7 Tg C (+81 %). The combined effect on all three seas grouped together is +11.7 Tg C ($-26$ %, i.e. a 26 % reduction in the regional sink).

### 3.4 Uncertainties and error propagation

Uncertainties and bias in the remote sensing data used to calculate $F$ could have a significant impact on the resultant $CO_2$ fluxes. To investigate the effect of known random errors in the input data sets, the published standard deviation for each data set was used to perturb the respective variable. These are 0.16 °C in $T_{\mathrm{skin}}$, 0.6 °C in $T_{\mathrm{fnd}}$ and $1.25\,\mathrm{m\,s^{-1}}$ in $U_{10}$. To investigate the effect of random fluctuations, each individual measurement was perturbed by a random number (noise) with a log-normal distribution, assuming all errors to be uncorrelated. The integrated fluxes for 2008 and 2009 were recalculated five times for each sea using the perturbed

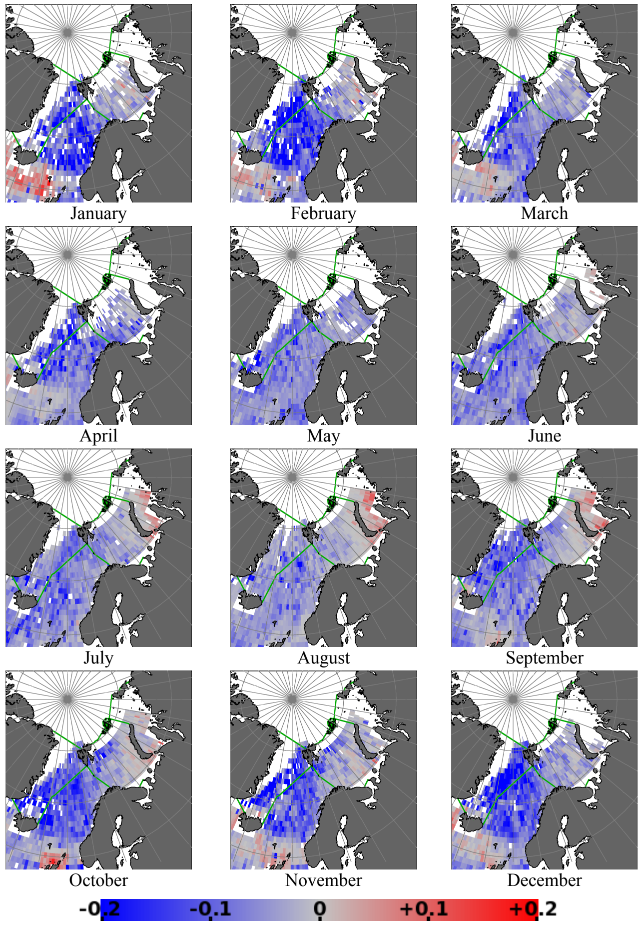


**Fig. 6.** Monthly mean sea–air flux of $CO_2$ in $\mathrm{g\,C\,m^{-2}\,day^{-1}}$ during 2008 and 2009 combined using the Nightingale et al. (2000) $k$ parameterization. Blue is absorbing, red is emitting, grey is land, white is no data.

data, and the standard deviation of integrated flux calculated, which then forms our estimate of the uncertainty due to random errors. All input data sets were perturbed simultaneously.

It is also possible that the input data contain a bias, e.g. due to poor cloud clearing leading to a cooler SST than expected, anomalous atmospheric correction over the Arctic, or the small number of cloud free data typically available in this region. This will have a proportionately much larger impact on the total error. $T_{\text{fnd}}$ has been found to have negligible bias globally (Donlon et al., 2011), but regional biases are evident. A specific challenge in this respect is the lack of in situ measurements in the Arctic regions that can be used to provide robust validation statistics. We took the precautionary approach of assuming all regional biases to equal the root mean square (rms) sum of the published bias (if any) and standard deviation of random errors in each case. These are $\sqrt{0.16^2+0.2^2}=0.26\,°\mathrm{C}$ in $T_{\text{skin}}$, $0.6\,°\mathrm{C}$ in $T_{\text{fnd}}$ (which has a published bias of zero) and $\sqrt{1.25^2+0.28^2}=1.28\,\mathrm{m\,s^{-1}}$ in $U_{10}$, and should be considered to be an upper estimate of the error due to bias. To investigate the effect of possible input data biases in $T_{\text{skin}}$, $T_{\text{fnd}}$ and $U_{10}$ on the integrated fluxes, each data set in turn was offset by this value and the resulting flux offset calculated. To prevent pixels being masked by $T_{\text{fnd}}$ exceeding $T_{skin}$, which generates an error in the algorithm, $T_{\text{fnd}}$ was offset negatively, while $T_{\text{skin}}$ and $U_{10}$ were offset positively.

All of these flux errors (the standard deviation due to random fluctuations and the flux offsets due to potential sources of bias) were assumed to be uncorrelated and hence were combined to give a cumulative rms error due to potential errors in the EO input data. This assumption is probably invalid for $T_{\text{fnd}}$ and $T_{\text{skin}}$, which we expect to co-vary, but again this approach sets an upper limit on the error.

For the remaining parameters in Eq. (3) we followed the analysis of Takahashi et al. (2009), adjusting the values to suit our regions of interest. In their discussion of errors, Takahashi et al. (2009) use $F=0.585\alpha(Sc)^{1/2}(U_{10})^2\,\Delta p\mathrm{CO_2}$. They quote an error of 30 % in the factor 0.585, which is actually an error in the $k$ algorithm used by Takahashi et al. (2009), an empirical wind-based algorithm similar to those of Nightingale et al. (2000) and Ho et al. (2006). However, Ho et al. (2011) quote errors in the $k$ algorithms of Nightingale et al. (2000) and Ho et al. (2006) of 20 %, so we use 20 % here. Takahashi et al. (2009) also quote errors of 10 % in the solubility and Schmidt number product $\alpha(Sc)^{1/2}$ and 0.9 µatm in $\Delta p\mathrm{CO_2}$, which converts to a percentage error of $100\times0.9\sqrt{\Delta p\mathrm{CO_2}}$. Assuming that these errors are independent, they combine to a percentage error in $F$ of $\sqrt{20^2+10^2+\left(100\times0.9\sqrt{\Delta p\mathrm{CO_2}}\right)}$ due to uncertainties in the method.

Results for the different error sources are shown in Table 8 for integrated fluxes calculated using the Nightingale et al. (2000) $k$ parameterization. The errors vary between seas, but in all cases the dominant error is that due to wind bias, comprising 67 to 82 % of the total error, and the error due to random fluctuations in the EO input data is negligible. For the Greenland and Barents seas, the next greatest error is that due to uncertainties in the method, which itself is dominated by the 20 % error in the $k$ parameterization.

## 4 Discussion

### 4.1 Comparison with previous work

Calculated annual integrated $CO_2$ fluxes for each of the three seas during 2008 and 2009 using Nightingale et al. (2000) and Ho et al. (2006) are shown in Table 9 and Fig. 12a, along with results from previous studies for comparison. The in situ measurements are summarised by Bates and Mathis (2009). Of the previous studies, Arrigo et al. (2010) and Nakaoka et al. (2006) use empirical wind-based $k$ parameterizations similar to Nightingale et al. (2000) and Ho et al. (2006), while

**Table 6.** Annual integrated $CO_2$ fluxes from the three seas using the $k$ parameterizations of Nightingale et al. (2000) and Ho et al. (2006). Errors are upper estimates, taken from Table 8.

| Sea | Area ($km^2$) | Annual integrated $CO_2$ flux (Tg C) | | | |
|---|---|---|---|---|---|
| | | Nightingale et al. (2000) | | Ho et al. (2006) | |
| | | 2008 | 2009 | 2008 | 2009 |
| Greenland | 1 080 210 | −37 ± 14 | −36 ± 14 | −37 ± 15 | −36 ± 14 |
| Barents | 1 349 030 | −9 ± 4 | −14 ± 6 | −9 ± 4 | −14 ± 6 |
| Kara | 760 450 | +2.9 ± 1.9 | +1.4 ± 0.9 | +2.8 ± 1.8 | +1.4 ± 0.9 |
| All seas | 3 189 690 | −43 ± 17 | −48 ± 19 | −44 ± 18 | −49 ± 20 |

**Table 7.** Effects of increased $T_{fnd}$ and $T_{skin}$, decreased salinity (freshening) and reduction in sea ice duration on annual integrated $CO_2$ flux using the $k$ parameterization of Nightingale et al. (2000).

| Parameter (unit) | Sensitivity (Tg C unit$^{-1}$) Greenland Sea | Barents Sea | Kara Sea | all seas | Effect of 2020 prediction (Tg C) Greenland Sea | Barents Sea | Kara Sea | all seas |
|---|---|---|---|---|---|---|---|---|
| $T_{fnd}$ and $T_{skin}$ (°C) | +7.8 | +11.1 | +3.2 | +22.1 | +5.0 | +7.3 | +2.1 | +14.5 |
| Salinity (PSU) | −8.6 | −12.4 | −4.0 | −25.0 | −0.87 | −1.24 | −0.41 | −2.52 |
| Ice duration (days) | −0.030 | −0.013 | −0.00028 | −0.043 | −0.20 | −0.11 | −0.022 | −0.33 |
| Combined | | | | | +4.0 | +6.0 | +1.7 | +11.7 |

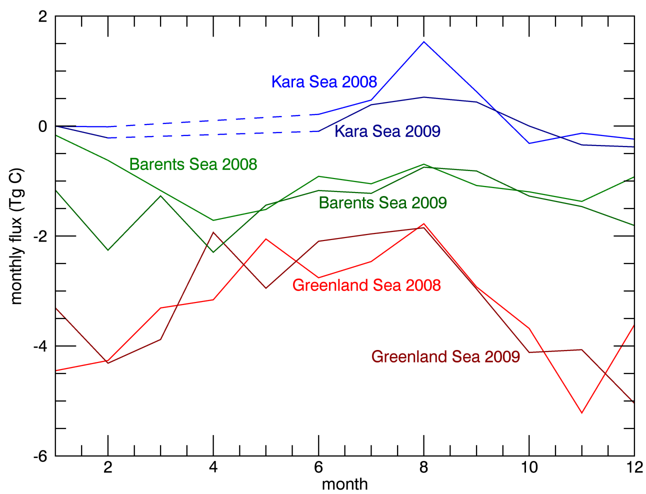


**Fig. 7.** Integrated monthly $CO_2$ fluxes over the three seas in 2008 and 2009 using the $k$ parameterization of Nightingale et al. (2000). The dashed sections of the Kara Sea graphs represent missing data in March, April and May caused by lack of EO data due to ice coverage. These are filled by linear interpolation of the mean Kara Sea $F$ between February and June.

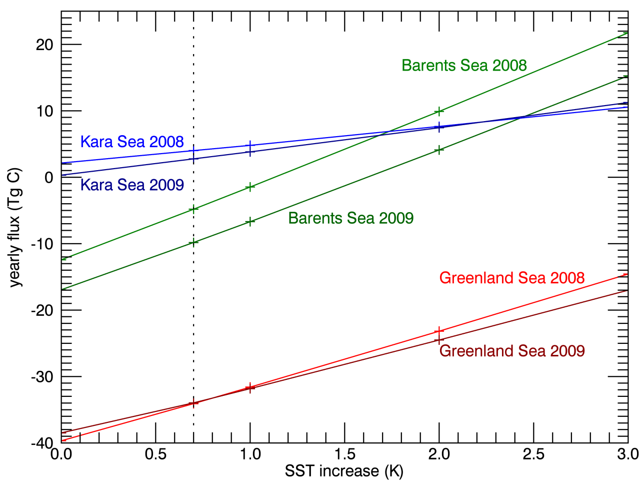


**Fig. 8.** Effect of increasing both $T_{fnd}$ and $T_{skin}$ on the integrated yearly $CO_2$ fluxes over the three seas in 2008 and 2009 using the $k$ parameterization of Nightingale et al. (2000). The ACIA (2005) prediction of 0.7 °C by 2020 is shown as a dotted line.

the others do not use a $k$ parameterization. Hence it is appropriate to compare our Nightingale et al. (2000) and Ho et al. (2006) data with data from these two studies.

Our values in the Greenland Sea are in good agreement with those of Arrigo et al. (2010), with a positive integrated flux difference (decrease in negative integrated flux) of around 1 Tg C. In the Barents Sea, both Arrigo et al. (2010) and the present work suggest values much less negative than previous in situ studies. Comparing our data with Arrigo et al. (2010), we find an integrated flux difference of around +13 Tg C, while the difference with in situ studies ranges from +33 to +66 Tg C. In the Kara Sea, all previous studies have found a small negative integrated flux but we find a small positive integrated flux. Compared with Arrigo et

**Table 8.** Estimation of the sensitivity of annual integrated $CO_2$ flux calculations to sources of input data uncertainty for the Nightingale et al. (2000) $k$ parameterization for each Arctic sea.

| Sea | Annual mean $\Delta pCO_2$ | Error due to method uncertainties (%) | Error due to fluctuations in $T_{skin}$, $T_{fnd}$ and $U_{10}$ (%) | Upper estimate of error due to bias (%) $T_{skin}$ | $T_{fnd}$ | $U_{10}$ | Upper estimate of total error (%) |
|---|---|---|---|---|---|---|---|
| Greenland | −67 | 22 | 0.5 | 4.5 | 1.3 | 32 | 39 |
| Barents | −13.6 | 23 | 0.2 | 22 | 3.7 | 33 | 47 |
| Kara | −3.5 | 34 | 0.2 | 34 | 1.1 | 44 | 65 |
| All seas | −29 | 23 | 0.5 | 11 | 2.0 | 31 | 40 |

**Table 9.** Mean annual sea–air integrated $CO_2$ flux in the three seas over 2008 and 2009, compared with those from previous studies and the years to which they refer. Values in bold use remote sensing data (Arrigo et al. (2010) also uses model data), others rely on in situ measurements or model data. Of the two values listed in our annual integrated $CO_2$ flux data, the first uses the $k$ parameterization of Nightingale et al. (2000), the second Ho et al. (2006).

| | | Previous studies | | |
|---|---|---|---|---|
| Sea | Annual $CO_2$ flux (Tg C) | Annual $CO_2$ flux (Tg C) | Measurement period | Reference |
| Greenland | **$-36 \pm 14$**<br>**$-37 \pm 14$** | **$-37.8 \pm 2.8$** | **1998–2003** | **Arrigo et al. (2010)** |
| Barents | **$-11 \pm 5$**<br>**$-11 \pm 5$** | $-70 \pm 27$<br>$-77 \pm 12$<br>$-67 \pm 15$<br>$-44 \pm 16$<br>**$-24.1 \pm 2.8$** | 1992–2001<br>1990–1999<br>1995–1997<br>1999<br>**1998–2003** | Nakaoka et al. (2006)<br>Omar et al. (2007)<br>Fransson et al. (2001)<br>Kaltin et al. (2002)<br>**Arrigo et al. (2010)** |
| Kara | **$+2.2 \pm 1.4$**<br>**$+2.1 \pm 1.4$** | $-1.0$<br>$-5.7$<br>**$-12.4 \pm 3.5$** | 1995–1997<br>1991 (model)<br>**1998–2003** | Fransson et al. (2001)<br>Anderson et al. (1998a, b)<br>**Arrigo et al. (2010)** |

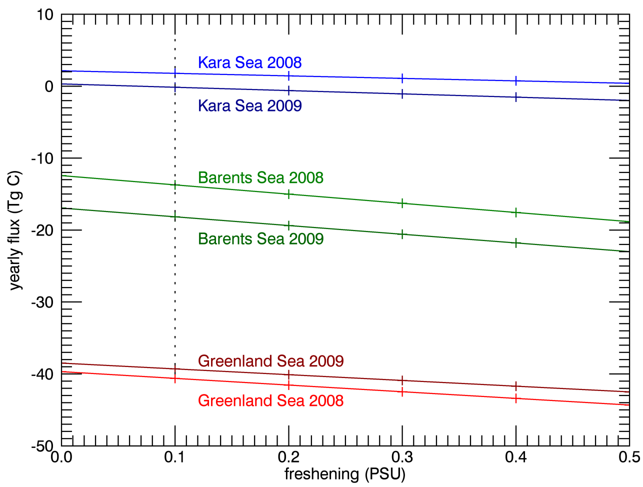


**Fig. 9.** Effect of freshening on the integrated yearly $CO_2$ fluxes over the three seas in 2008 and 2009 using the $k$ parameterization of Nightingale et al. (2000). The ACIA (2005) prediction of 0.1 PSU by 2020 is shown as a dotted line.

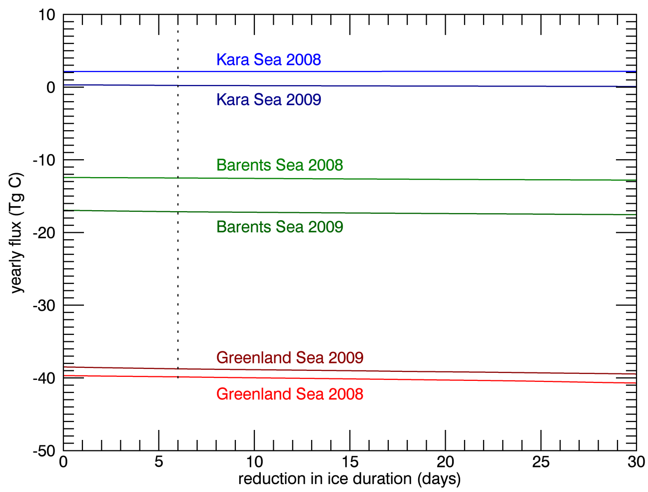


**Fig. 10.** Effect of changing sea ice duration on the integrated yearly $CO_2$ fluxes over the three seas in 2008 and 2009 using the k parameterization of Nightingale et al. (2000). The ACIA (2005) prediction of a 6-day reduction by 2020 is shown as a dotted line.

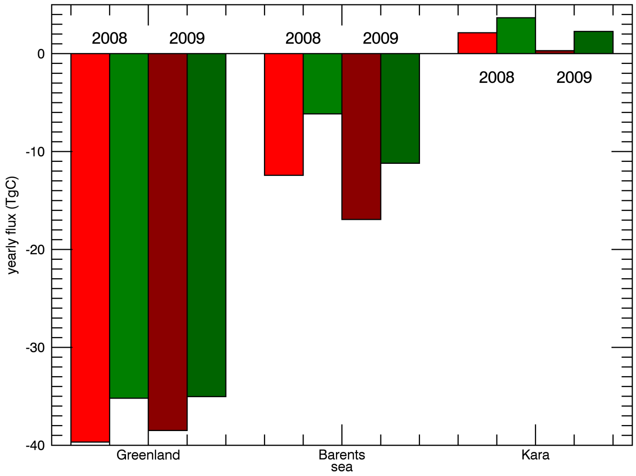


**Fig. 11.** Combined effect of the changes predicted for 2020 (0.7 °C temperature increase, 0.1 PSU freshening and 6-day decrease in sea ice duration) on the integrated yearly $CO_2$ fluxes over the three seas in 2008 and 2009 using the $k$ parameterization of Nightingale et al. (2000). Red bars indicate the original fluxes, green bars the 2020 prediction.

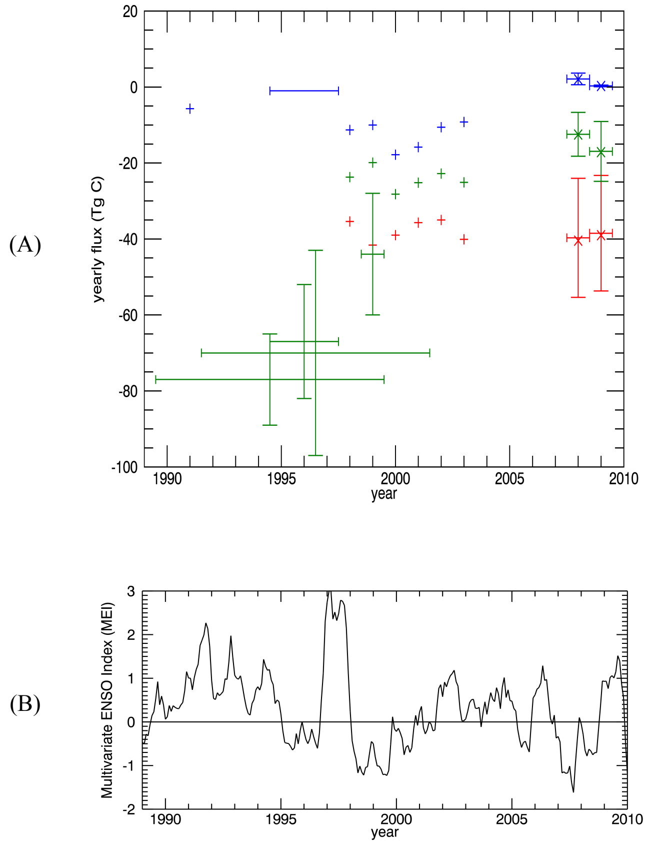


**Fig. 12. (A)** $CO_2$ fluxes in the three seas measured in previous studies and the current study (2008 and 2009). Red denotes the Greenland Sea, green the Barents Sea and blue the Kara Sea. Vertical error bars denote the stated uncertainty, if any. Horizontal error bars denote the years over which data were collected. In the case of 2008 and 2009 data, vertical error bars denote the $k$ parameterization of Nightingale et al. (2000), "$x$" (without error bars) that of Ho et al. (2006). Errors in Ho et al. (2006) are almost identical to those in Nightingale et al. (2000). Year labels mark the centre of the year. **(B)** The Multivariate ENSO Index (MEI), a measure of the strength of El Niño.

al. (2010) we find an integrated flux difference of around +14 Tg C, while the difference with in situ studies ranges from +3 to +8 Tg C.

Care should be taken when interpreting the Kara Sea data, since the Takahashi et al. (2009) data set excludes large parts of the Kara Sea. In the summer months when these parts are ice free, a large proportion of the Kara Sea integrated flux will be an estimate based on the mean flux from a much smaller proportion. This is acceptable for the current sensitivity study, but not for an estimate of the integrated $CO_2$ flux from the Kara Sea.

When comparing annual integrated sea $CO_2$ fluxes from this study with those from other studies, it should be noted that the purpose of this study is not to give values for the annual integrated $CO_2$ flux but to investigate the sensitivity of this flux to various perturbations, so this comparison is given more as a "reality check" than a claim to improve on previous estimates. Differences in the definition of the sea boundaries by Arrigo et al. (2010) also confound direct comparison. They define the seas as segments of the Arctic with a southern boundary at 66°33′39″ N. It should also be borne in mind that the Arctic seas have changed drastically since 2007, especially in summer ice extent (Stroeve et al., 2008; Wang and Overland, 2009), so we might expect differences from pre-2007 studies. The previous studies all take their data from the late 1990s or early 2000s and are presented along with the values from this study in Table 9.

Notwithstanding these issues, none of our values seem inconsistent with previous data. When the various estimates are ordered (see Fig. 12a), the largest step change occurs between the Barents and Kara Sea values of Arrigo et al. (2010) and the previous in situ studies. The Barents Sea data taken as a whole suggest a rising trend (i.e. a reducing sink) in annual integrated sea–air $CO_2$ flux. It is interesting to note from Fig. 12a that the data of Arrigo et al. (2010) appear to follow a rising trend with strong outliers in 1998 (all seas) and 1999 (Barents and Kara seas). These outliers may have been affected by the 1997–1998 El Niño, which was the strongest El Niño since 1983 (Wolter, 2012; Wolter and Timlin, 1998). Many authors, e.g. Liu et al. (2004), have postulated links between conditions in the Arctic and El Niño, with a delay of about three months between an El Niño event and the response in the Arctic. The Multivariate El Niño Southern Oscillation Index (MEI) is shown in Fig. 12b for comparison (Wolter and Timlin, 1998).

### 4.2 Effects of partial ice cover

The work of Loose et al. (2009) and Else et al. (2011) suggests that increased water turbulence may enhance the flux in marginal ice zones over a simple proportionality to open water area, while Woolf (2005) suggests that adjacent open waters with low fetch might have reduced transfer velocity. Though we have included a parameterization suggested by Loose et al. (2009), this is clearly a gross simplification. The marginal ice zones are complex and merit their own study, but this work takes an intentionally simple approach to transfer velocity, concentrating more on the driving concentration difference, which is affected by thermal and ice melt effects. In all but the Kara Sea, ice-covered regions are smaller than open ocean areas for most of the year (annual mean ice cover 27 %, 16 % and 57 % for the Greenland, Barents and Kara seas), and much of this will be fast ice. The Kara Sea has by far the smallest magnitude of $CO_2$ flux of the three seas due to its low concentration difference, so contributes very little to the integrated regional flux. Hence the effect of neglected processes within marginal ice zones is likely to be a small correction to the integrated regional flux.

### 4.3 Effects of increased temperature, freshening and reduction in sea ice duration

The annual integrated $CO_2$ flux from each sea shows strong temperature dependence in all seas, especially in the Barents Sea (Table 8). The entire integrated flux from the Greenland and Barents seas in Table 7 can be negated by warmings of 5 and 1 °C, respectively, while the small positive integrated flux from the Kara Sea can be doubled by a warming of 0.7 °C (Sect. 3.3). The integrated flux from the region as a whole can be negated by a warming of 2 °C. The sensitivity of the integrated $CO_2$ flux in the Barents Sea to warming is 1.4 times that in the Greenland Sea, and 3.4 times that in the Kara Sea.

The dependence of the integrated $CO_2$ flux on salinity is also strong, but in the opposite direction. The integrated flux from the Greenland and Barents seas can be doubled by freshenings of 4.2 and 0.9 PSU, respectively, while the Kara Sea integrated flux can be negated by a freshening of 0.5 PSU (Sect. 3.3). The integrated $CO_2$ flux from the region as a whole can be doubled by a freshening of 1.8 PSU. The sensitivity of the Barents Sea integrated $CO_2$ flux to freshening is once again the greatest, 1.4 times that in the Greenland Sea and 3.1 times that in the Kara Sea.

The sensitivity of the integrated $CO_2$ flux to reduction in sea ice duration is surprisingly weak. Even a 30-day reduction only affects the annual integrated fluxes by a maximum of $-0.9$ Tg C (2.5 %) in the Greenland Sea, $-0.39$ Tg C (3.5 %) in the Barents Sea and $-0.018$ Tg C (0.8 %) in the Kara Sea. It may be that to give a realistic reduction in sea ice extent, an additional factor needs to be included. Studies such as ACIA (2005) frequently predict changes in ice extent, but to implement such a change directly requires a means of deciding which ice to remove. Future work could benefit from information on sea ice thickness, which would allow the removal of the thinnest ice until the required extent is achieved.

The negative integrated $CO_2$ flux changes in the Kara Sea due to reduced sea ice duration may appear to be counterintuitive, since an emitting sea that has less ice cover should emit more strongly. However, this can be explained by the fact that the Kara Sea has areas that emit $CO_2$ and areas that absorb; see Fig. 5 and Sect. 4.5. If the decrease in emission due to more absorbing surface being exposed is greater than the increase due to more emitting surface being exposed, then the overall emission is reduced.

### 4.4 Impact of surface biology on the *k* parameterization

Autotrophy on Arctic shelves fuelled by inputs of nutrients both from rivers and by on-shelf transport gives the potential for significant biological $CO_2$ uptake and modification of air–sea gas exchange. Surfactants such as polysaccharides, lipids and proteins deriving from phytoplankton (Žutić et al., 1981; Liss and Duce, 2005; Gašparović et al., 1998) suppress $k$ by acting as a monolayer physical barrier and by modifying sea surface hydrodynamics, reducing surface roughness and turbulent energy transfer. Based on broad correlations of surfactant with primary productivity, strong spatial and seasonal gradients in $k$ should be expected (e.g. Goldman et al., 1988), especially in the Kara Sea given its large terrestrial freshwater supply. Although there are currently no data on the occurrence of biological surfactant in Arctic waters, there have previously been attempts to use EO data to infer open ocean distributions of surfactant (Liu et al., 2000; Lin et al., 2002) and the implications for gas exchange (Tsai and Liu, 2003). The latter authors used $\Delta p CO_2$ climatologies and EO derived estimates of $U_{10}$, sea surface temperature and chlorophyll $a$ to infer surfactant control on global air–sea $CO_2$ exchange. Their data imply measurable $k$ suppression beyond a PP of 25 g C m$^{-2}$ month$^{-1}$ (820 mg C m$^{-2}$ day$^{-1}$) (Tsai and Liu, 2003). Surfactant suppression of $k$ has also been estimated more directly, both in the laboratory and in other field locations, the typical range of $k$ suppression being 5–60 %, (Goldman et al., 1988; Frew et al., 1990; Bock et al., 1999; Salter et al., 2011). A deliberate surfactant release in the NE Atlantic found 5–55 % $k$ suppression for $U_{10}$ in the range 7.2–10.7 m s$^{-1}$ (Salter et al., 2011). Table 3 shows that the interquartile range of wind speeds (Q1 to Q3 in Table 3) overlaps with this range, indicating frequent occurrence of wind speeds in this range, for 9 months of the year in the Greenland Sea, all 12 months in the Barents Sea and 6 months in the Kara Sea, hence substantial modification of $k$ seems possible.

Figure 13 is a cumulative histogram of PP for the three seas, in which the vertical axis shows the proportion of the clear sea area with a given PP (shown on the horizontal

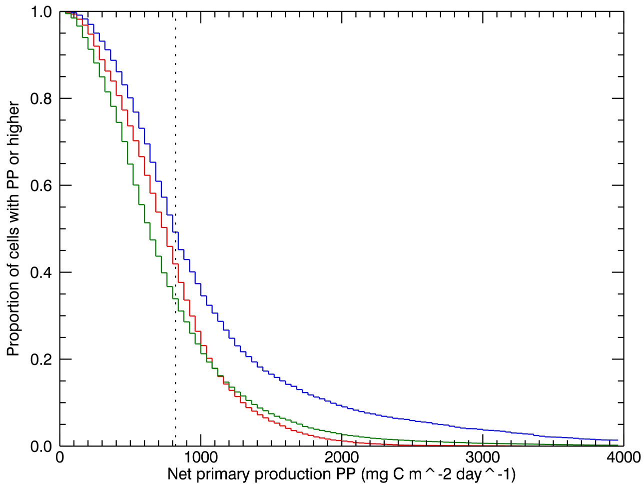


**Fig. 13.** Cumulative histogram of net primary production showing the proportion of clear sea area with a given net primary production or higher. The dotted line represents the threshold of slick formation. Red is the Greenland Sea, green the Barents Sea and blue the Kara Sea.

axis) or higher. This enables a crude estimate of the scale of $k$ suppression by surfactant assuming strong PP-surfactant correlations and shows the Kara Sea to have a consistently higher proportion of high PP than the other seas, for which PP is broadly similar. The proportions exceeding 820 mg C $m^{-2}$ $day^{-1}$ are: Greenland Sea 42 %; Barents Sea 34 %; Kara Sea 49 %.

We may conclude from the above that using $k$ parameterizations explicitly incorporating surface roughness, derived for example from satellite backscatter data (e.g. Fangohr and Woolf, 2007), should give a more accurate representation of Arctic $CO_2$ exchange than those based on wind speed alone, e.g. Nightingale et al. (2000). Nevertheless, the $CO_2$ exchange fluxes calculated here using Fangohr and Woolf (2007) are consistently of a greater magnitude than those calculated using Nightingale et al. (2000) by a factor of about 1.75. This indicates a problem with the Fangohr and Woolf (2007) algorithm that causes it to overestimate $F$, and recent work by Goddijn-Murphy (2012) has identified a calibration issue for $k_d$; the calibration of $k_b$ is still unknown. Once such issues are resolved, approaches of the type proposed by Fangohr and Woolf (2007) have the potential to enable more realistic parameterization and consequently improved $CO_2$ exchange estimates for this region.

First inspection of our altimeter-based estimates of $U_{10}$, which derive from surface roughness measurements, implies that they should be largely unaffected by the above issues. However, the ESA data processing chain corrects the estimated wind speeds using modelled wind speed data for the same time and location. Therefore, despite their origin in surface roughness data, $k$ estimates deriving from these wind speed estimates are likely to be biased high in regions of high biological activity.

### 4.5 Potential impact of terrestrial DOC inputs on $CO_2$ exchange fluxes

Marginal shelves are extremely important to Arctic Ocean biogeochemistry due to their large area (> 53 % of the total) and the scale of terrestrial inputs. The Arctic receives ∼ 10 % of global river discharge and inputs are increasing by 8 $km^3$ $yr^{-1}$ due to snow cover and soil ice losses (Dai et al., 2009). Most freshwater input is to the Kara Sea, via the Ob and Yenisey rivers, which along with the adjacent Barents Sea, borders the large Eurasian watershed (Fig. 1). This extends south as far as 45°N and covers $\sim 5.5 \times 10^6$ $km^2$ inclusive of the world's largest peat bog, which may contain 50 % of global soil carbon (McGuire et al., 2002).

It is estimated that 25–36 Tg C $yr^{-1}$ is delivered to the Arctic Ocean via rivers, of which > 90 % is dissolved (DOC) (Raymond et al., 2007; Makkaveev et al., 2010); this is ∼ 10–15 % of the global terrigenous DOC supply (Stein and MacDonald, 2004). Terrestrial DOC delivery to the Kara Sea is especially high; the Ob and Yenisey rivers combined supply it with ∼ 8.6 Tg C $yr^{-1}$ as DOC (Lobbes et al., 2000), ∼ 34 % of all river-derived DOC in the Arctic Ocean. Moreover, the river water flux to the Arctic is increasing by ∼ 8 $km^3$ $yr^{-1}$ (Dai et al., 2009) and a progressive increase in the depth of seasonal permafrost melting in the Siberian Arctic is potentially mobilising 'old' DOM stores (Zhang et al., 2005).

The biogeochemical fate of river-derived DOC in the Arctic Ocean is thus potentially important to the regional carbon budget. DOC remineralisation to $CO_2$ on Arctic shelves has the potential to offset autotrophic $CO_2$ uptake to some degree, though typically strong spatial and seasonal signals in continental shelf $CO_2$ dynamics complicate the estimation of the autotrophic-heterotrophic balance. Although a strong halocline and rapid surface transport may enable > 50 % of terrigenous DOC to escape significant remineralisation on Arctic shelves (Opsahl et al., 1999), removal rate constants are high (Letscher et al., 2011) and 30–70 % respiration of river-borne DOC has been observed in the Beaufort Gyre (Hansell et al., 2009; Cooper et al., 2005). Globally it is estimated that ∼ 50 % of river-borne DOC is returned to the troposphere as $CO_2$ in estuaries (Laruelle et al., 2011; Cai, 2011).

Using this figure, assuming that all DOC remineralisation in the Arctic is restricted to coastal shelves and using the DOC delivery estimates above (Raymond et al., 2007; Makkaveev et al., 2010) gives a potential annual $CO_2$ outgassing integrated flux from Arctic shelves of 11–16 Tg C $yr^{-1}$ (2–3 g C $m^{-2}$ $yr^{-1}$). For comparison, average annual sea–air integrated fluxes from Table 6 are −11 Tg C $yr^{-1}$ (−8 g C $m^{-2}$ $yr^{-1}$) for the Barents Sea and +2.2 Tg C $yr^{-1}$ (+3 g C $m^{-2}$ $yr^{-1}$) for the Kara Sea. Rates on individual shelves will, however, certainly vary due to differences in freshwater inputs. Given that the Kara Sea receives ∼34 % of all DOC river inputs to the Arctic Ocean (Lobbes et al., 2000), it could potentially return 3.7–5.4 $Tg\,C\,yr^{-1}$ (4.9–7.2 $g\,C\,m^{-2}\,yr^{-1}$) of $CO_2$ via DOC remineralisation, significantly larger than our estimate of integrated Kara Sea flux. This provides a potential explanation for our result that the Kara Sea has very small $CO_2$ flux compared to the Greenland and Barents seas, despite having high primary productivity. A large biological $CO_2$ drawdown could be offset by a similarly large outgassing due to DOC remineralization, leaving a small net flux.

## 5 Conclusions

This study has shown that integrated $CO_2$ fluxes in three Arctic seas are strongly sensitive to changes in temperature and salinity, but are much less sensitive to changes in sea ice duration. All become smaller $CO_2$ sinks (or larger sources) at higher temperatures and larger $CO_2$ sinks (or smaller sources) at lower salinities and to a lesser extent at reduced sea ice duration. Predictions of the relative magnitudes of these changes up to 2020 suggest that the temperature effect will dominate, in which case future changes in climate have the potential to decrease the collective function of these seas as a sink of atmospheric $CO_2$. The predicted effect (26 % reduction in the overall sink over 11.5 yr) would, if it continued at the same rate, result in the region ceasing to be a net sink in the mid 2050s. Different combinations of warming, freshening and sea ice reduction will of course have different effects.

In terms of absolute changes in integrated $CO_2$ flux, the Barents Sea is the most sensitive of the three seas to warming and freshening and the Greenland Sea is the most sensitive to sea ice reduction. Our results suggest that sea ice reduction alone has by far the smallest effect (although this leads to open water and thus further warming of the ocean surface layer); therefore, we conclude that the effect of future changes in climate on the integrated $CO_2$ flux will be largest in the Barents Sea. The Kara Sea integrated $CO_2$ flux is both the smallest in magnitude and the least affected by the three changes.

This work has shown that the integrated $CO_2$ fluxes are relatively insensitive to changes in ice duration. However, use of daily ice thickness data would allow a more detailed analysis of these effects. Finally, the high biological activity within these seas, especially within the Kara Sea, suggests that future studies should avoid using purely wind-based parameterizations of the gas transfer velocity, as these are likely to overestimate the $CO_2$ flux in these regions. If a wind-based parameterization is used, an attempt should be made to include this issue in uncertainty estimates.

*Acknowledgements.* The authors would like to acknowledge and thank Karen Anderson, who co-supervised the work of R. D. Cowling during his MSc studies; these studies provided the basis for this work. The authors thank P. Nightingale for helpful discussions throughout this study. This work was partially funded by the following grants: the ESA Support to Science Element (STSE) Fellowship project "Open ocean and Coastal $CO_2$ fluxes from Envisat and Sentinel 3 in support of global carbon cycle monitoring (OC-flux)"; the UK NERC Strategic marine research programme Oceans 2025; the UK National Centre for Earth Observation (NCEO) marine carbon theme and seed funding from the Plymouth Marine Laboratory and ESA STSE project "OceanFlux Greenhouse Gases" (contract 4000104762/11/I-AM). All Earth observation data processing and re-projection was achieved using resources kindly provided by the UK NERC Observation Data Acquisition and Analysis Service (NEODAAS).

Edited by: C. Garbe

## References

ACIA: Arctic Climate Impact Assessment, Cambridge University Press, 1042 pp., 2005.

Anderson, L. G., Olsson, K., and Chierici, M.: A carbon budget for the Arctic Ocean, Global Biogeochem. Cy., 12, 455–465, 1998a.

Anderson, L. G., Olsson, K., Jones, E. P., Chierici, M., and Fransson, A.: Anthropogenic carbon dioxide in the Arctic Ocean: Inventory and sinks, J. Geophys. Res., 103, 27707–27727, 1998b.

Arrigo, K. R., van Dijken, G., and Pabi, S.: Impact of a shrinking Arctic ice cover on marine primary production, Geophys. Res. Lett., 35, L19603, doi:10.1029/2008GL035028, 2008.

Arrigo, K. R., Pabi, S., van Dijken, G. L., and Maslowski, W.: Air-sea flux of $CO_2$ in the Arctic Ocean, 1998–2003, J. Geophys. Res., 115, G04024, doi:10.1029/2009JG001224, 2010.

Bates, N. R. and Mathis, J. T.: The Arctic Ocean marine carbon cycle: evaluation of air-sea $CO_2$ exchanges, ocean acidification impacts and potential feedbacks, Biogeosciences, 6, 2433–2459, doi:10.5194/bg-6-2433-2009, 2009.

BEAM: ESA Earth observation toolbox and development platform, version 4.8: http://www.brockmann-consult.de/cms/web/beam, 2010.

Birks, A.: AATSR products handbook, Issue 2.2, ESA Publications Division, 2007.

Bock, E. J., Hara, T., Frew, N. M., and McGillis, W. R.: Relationship between air sea gas transfer and short wind waves, J. Geophys. Res., 104, 25821–25831, 1999.

Boutin, J., Etcheto, J., Merlivat, L., and Rangama, Y.: Influence of gas exchange coefficient parameterisation on seasonal and regional variability of $CO_2$ air-sea fluxes, Geophys. Res. Lett., 29, 1182, doi:10.1029/2001GL013872, 2002.

Cai, W. J.: Coastal ocean carbon paradox: $CO_2$ sinks or sites of terrestrial carbon incineration, Annu. Rev. Mar. Sci., 3, 123–145, 2011.

Cooper, L. W., Benner, R., McClelland, J. W., Peterson, B. J., Holmes, R. M., Raymond, P. A., Hansell, D. A., Grebmeier, J. M., and Codispoti, L. A.: Linkages among runoff, dissolved organic carbon, and the stable oxygen isotope composition of seawater and other water mass indicators in the Arctic Ocean, J. Geophys. Res., 110, G02013, doi:10.1029/2005JG000031, 2005.

Dai, A., Qian, T., Trenberth, K. E., and Milliman, J. D.: Changes in continental freshwater discharge from 1948 to 2004, J. Climate, 22, 2773–2792, 2009.

Denman, K. L., Brasseur, G., Chidthaisong, A., Ciais, P., Cox, P. M., Dickinson, R. E., Hauglustaine, D., Heinze, C., Holland, E., Jacob, D., Lohmann, U., Ramachandran, S., da Silva Dias, P. L., Wofsy, S., and Zhang, X.: Couplings between changes in the climate system and biogeochemistry., in: Climate Change 2007: The Physical Science Basis. Contribution of Working Group I to the Fourth Assessment Report of the Intergovernmental Panel on Climate Change, edited by: Solomon, S., Qin, D., Manning, M., Chen, Z., Marquis, M., Averyt, K., Tignor, M., and Miller, H., Cambridge University Press, Cambridge, United Kingdom and New York, NY, USA, 2007.

Donlon, C., Robinson, I., Casey, K. S., Vazquez-Cuervo, J., Armstrong, E., Arino, O., Gentemann, C., May, D., LeBorgne, P., and Piollé, J.: The global ocean data assimilation experiment high-resolution sea surface temperature pilot project, B. Am. Meteorol. Soc., 88, 1197–1213, 2007.

Donlon, C. J., Martin, M., Stark, J., Roberts-Jones, J., Fiedler, E., and Wimmer, W.: The Operational Sea Surface Temperature and Sea Ice Analysis (OSTIA) system, Remote Sens. Environ., 116, 140–158, doi:10.1016/j.rse.2010.10.017, 2011.

Edwards, T., Browning, R., Delderfield, J., Lee, D. J., and Lidiard, K. A.: The along track scanning radiometer-Measurement of sea-surface temperature from ERS-1, J. Brit. Inter. Soc., 43, 160–180, 1990.

Else, B. G. T., Papakyriakou, T. N., Granskog, M. A., and Yackel, J. J.: Observations of sea surface $fCO_2$ distributions and estimated air-sea $CO_2$ fluxes in the Hudson Bay region (Canada) during the open water season, J. Geophys. Res., 113, C08026, doi:10.1029/2005JG000031, 2008.

Else, B. G. T., Papakyriakou, T. N., Galley, R. J., Drennan, W. M., Miller, L. A., and Thomas, H.: Wintertime $CO_2$ fluxes in an Arctic polynya using eddy covariance: Evidence for enhanced air-sea gas transfer during ice formation, J. Geophys. Res.-Oceans (1978–2012), 116, C00G03, doi:10.1029/2010JC006760, 2011.

Fangohr, S. and Woolf, D. K.: Application of new parameterizations of gas transfer velocity and their impact on regional and global marine $CO_2$ budgets, J. Mar. Syst., 66, 195–203, 2007.

Faugère, Y., Ollivier, A., Zanifé, O. Z., Scharroo, R., Martini, A., Roca, M., and Femenias, P.: An operational correction for the RA2 side A USO anomaly: Methods and performance assessment, ESA Symposium 2007, Montreux, Switzerland, 2007.

Fransson, A., Chierici, M., Anderson, L. G., Bussmann, I., Kattner, G., Peter Jones, E., and Swift, J. H.: The importance of shelf processes for the modification of chemical constituents in the waters of the Eurasian Arctic Ocean: implication for carbon fluxes, Cont. Shelf Res., 21, 225–242, 2001.

Frew, N. M., Goldman, J. C., Dennett, M. R., and Johnson, A. S.: Impact of phytoplankton-generated surfactants on air-sea gas exchange, J. Geophys. Res., 95, 3337–3352, 1990.

Gašparović, B., Kozarac, Z., Saliot, A., Ćosović, B., and Moebius, D.: Physicochemical characterization of natural and ex-situ reconstructed sea-surface microlayers, J. Colloid Interf. Sci., 208, 191–202, 1998.

Goddijn-Murphy, L. M., Woolf, D. K., and Marandino, C.: Space-based retrievals of air-sea gas transfer velocities using altimeters; calibration for dimethyl sulfide, J. Geophys. Res., 117, C08028, doi:10.1029/2011JC007535, 2012.

Goldman, J. C., Dennett, M. R., and Frew, N. M.: Surfactant effects on air-sea gas exchange under turbulent conditions, Deep-Sea Res., 35, 1953–1970, 1988.

Hansell, D. A., Carlson, C. A., Repeta, D. J., and Schlitzer, R.: Dissolved organic matter in the ocean: A controversy stimulates new insights, Oceanography, 22, 202–211, 2009.

Ho, D. T., Law, C. S., Smith, M. J., Schlosser, P., Harvey, M., and Hill, P.: Measurements of air-sea gas exchange at high wind speeds in the Southern Ocean: Implications for global parameterizations, Geophys. Res. Lett., 33, 16611, doi:10.1029/2006GL026817, 2006.

Ho, D. T., Wanninkhof, R., Schlosser, P., Ullman, D. S., Hebert, D., and Sullivan, K. F.: Toward a universal relationship between wind speed and gas exchange: Gas transfer velocities measured with 3He/SF6 during the Southern Ocean Gas Exchange Experiment, J. Geophys. Res., 116, C00F04, doi:10.1029/2010JC006854, 2011.

International Hydrographic Organization: Limits of oceans and seas, International Hydrographic Organization, 1953.

Kaltin, S., Anderson, L. G., Olsson, K., Fransson, A., and Chierici, M.: Uptake of atmospheric carbon dioxide in the Barents Sea, J. Mar. Syst, 38, 31–45, 2002.

Kettle, H. and Merchant, C. J.: Systematic errors in global air-sea $CO_2$ flux caused by temporal averaging of sea-level pressure, Atmos. Chem. Phys., 5, 1459–1466, doi:10.5194/acp-5-1459-2005, 2005.

Kettle, H., Merchant, C. J., Jeffery, C. D., Filipiak, M. J., and Gentemann, C. L.: The impact of diurnal variability in sea surface temperature on the central Atlantic air-sea $CO_2$ flux, Atmos. Chem. Phys., 9, 529–541, doi:10.5194/acp-9-529-2009, 2009.

Kwok, R., Cunningham, G. F., Wensnahan, M., Rigor, I., Zwally, H. J., and Yi, D.: Thinning and volume loss of the Arctic Ocean sea ice cover: 2003–2008, J. Geophys. Res., 114, C07005, doi:10.1029/2009JC005312, 2009.

Laruelle, G. G., Dürr, H. H., Slomp, C. P., and Borges, A. V.: Evaluation of sinks and sources of $CO_2$ in the global coastal ocean using a spatially-explicit typology of estuaries and continental shelves, Geophys. Res. Lett., 37, L15607, doi:10.1029/2010GL043691, 2011.

Letscher, R. T., Hansell, D. A., and Kadko, D.: Rapid removal of terrigenous dissolved organic carbon over the Eurasian shelves of the Arctic Ocean, Mar. Chem., 123, 78–87, 2011.

Lin, I. I., Wen, L. S., Liu, K. K., Tsai, W. T., and Liu, A. K.: Evidence and quantification of the correlation between radar backscatter and ocean colour supported by simultaneously acquired in situ sea truth, Geophys. Res. Lett., 29, 102–101, 2002.

Liss, P. S. and Duce, R. A.: The sea surface and global change, Cambridge Univ. Pr., 2005.

Liu, A. K., Wu, S. Y., Tseng, W. Y., and Pichel, W. G.: Wavelet analysis of SAR images for coastal monitoring, Can. J. Remote Sens., 26, 494–500, 2000.

Liu, J., Curry, J. A., and Hu, Y.: Recent Arctic sea ice variability: Connections to the Arctic Oscillation and the ENSO, Geophys. Res. Lett., 31, L09211, doi:10.1029/2004GL019858, 2004.

Lobbes, J. M., Fitznar, H. P., and Kattner, G.: Biogeochemical characteristics of dissolved and particulate organic matter in Russian rivers entering the Arctic Ocean, Geochim. Cosmochim. Ac., 64, 2973–2983, 2000.

Loose, B., McGillis, W. R., Schlosser, P., Perovich, D., and Takahashi, T.: Effects of freezing, growth, and ice cover on gas transport processes in laboratory seawater experiments, Geophys. Res. Lett., 36, L05603, doi:10.1029/2008GL036318, 2009.

Makkaveev, P. N., Stunzhas, P. A., Mel'nikova, Z. G., Khlebopashev, P. V., and Yakubov, S. K.: Hydrochemical characteristics of the waters in the western part of the Kara Sea, Oceanology, 50, 688–697, 2010.

McGillis, W. R. and Wanninkhof, R.: Aqueous $CO_2$ gradients for air–sea flux estimates, Mar. Chem., 98, 100–108, 2006.

McGuire, A. D., Wirth, C., Apps, M., Beringer, J., Clein, J., Epstein, H., Kicklighter, D. W., Bhatti, J., Chapin Iii, F. S., and Groot, B.: Environmental variation, vegetation distribution, carbon dynamics and water/energy exchange at high latitudes, J. Veg. Sci., 13, 301–314, 2002.

Nakaoka, S. I., Aoki, S., Nakazawa, T., Hashida, G., Morimoto, S., Yamanouchi, T., and Yoshikawa-Inoue, H.: Temporal and spatial variations of oceanic $p\mathrm{CO}_2$ and air–sea $CO_2$ flux in the Greenland Sea and the Barents Sea, Tellus B, 58, 148–161, 2006.

Nightingale, P. D., Malin, G., Law, C. S., Watson, A. J., Liss, P. S., Liddicoat, M. I., Boutin, J., and Upstill-Goddard, R. C.: In situ evaluation of air-sea gas exchange parameterizations using novel conservative and volatile tracers, Global Biogeochem. Cy., 14, 373–387, 2000.

O'Carroll, A. G., Eyre, J. R., and Saunders, R. W.: Three-way error analysis between AATSR, AMSR-E, and in situ sea surface temperature observations, J. Atmos. Ocean. Tech., 25, 1197–1207, 2008.

Omar, A. M., Johannessen, T., Olsen, A., Kaltin, S., and Rey, F.: Seasonal and interannual variability of the air-sea $CO_2$ flux in the Atlantic sector of the Barents Sea, Mar. Chem., 104, 203–213, 2007.

Opsahl, S., Benner, R., and Amon, R. M. W.: Major flux of terrigenous dissolved organic matter through the Arctic Ocean, Limnol. Oceanogr., 44, 2017–2023, 1999.

Pabi, S., van Dijken, G. L., and Arrigo, K. R.: Primary production in the Arctic Ocean, 1998–2006, J. Geophys. Res., 113, C08005, doi:10.1029/2007JC004578, 2008.

Polyakov, I. V., Timokhov, L. A., Alexeev, V. A., Bacon, S., Dmitrenko, I. A., Fortier, L., Frolov, I. E., Gascard, J. C., Hansen, E., and Ivanov, V. V.: Arctic Ocean warming contributes to reduced polar ice cap, J. Phys. Oceanogr., 40, 2743–2756, 2010.

Purkey, S. G. and Johnson, G. C.: Warming of global abyssal and deep Southern Ocean waters between the 1990s and 2000s: contributions to global heat and sea level rise budgets, J. Climate, 23, 6336–6351, 2010.

Queffeulou, P., Benramy, A., and Croize-Fillon, D.: Analysis of seasonal wave height anomalies from satellite data over the global oceans, ESA Living Planet Symposium, 2010.

Raymond, P. A., McClelland, J. W., Holmes, R. M., Zhulidov, A. V., Mull, K., Peterson, B. J., Striegl, R. G., Aiken, G. R., and Gurtovaya, T. Y.: Flux and age of dissolved organic carbon exported to the Arctic Ocean: A carbon isotopic study of the five largest arctic rivers, Global Biogeochem. Cy., 21, GB4011, doi:10.1029/2007GB002934, 2007.

Rosmorduc, V., Benveniste, J., Lauret, O., Maheu, C., Milagro, M., and Picot, N.: Radar Altimetry Tutorial: http://www.altimetry.info last access: September 2009.

Rysgaard, S., Glud, R. N., Sejr, M. K., Bendtsen, J., and Christensen, P. B.: Inorganic carbon transport during sea ice growth and decay: A carbon pump in polar seas, J. Geophys. Res., 112, C03016, doi:10.1029/2006JC003572, 2007.

Salter, M. E., Upstill-Goddard, R. C., Nightingale, P. D., Archer, S. D., Blomquist, B., Ho, D. T., Huebert, B., Schlosser, P., and Yang, M.: Impact of an artificial surfactant release on air-sea gas fluxes during Deep Ocean Gas Exchange Experiment II, J. Geophys. Res., 116, C11016, doi:10.1029/2011JC007023, 2011.

Sarmiento, J. L. and Gruber, N.: Ocean biogeochemical dynamics, Cambridge Univ Press, 2006.

Smyth, T. J., Tilstone, G. H., and Groom, S. B.: Integration of radiative transfer into satellite models of ocean primary production, J. Geophys. Res., 110, C10014, doi:10.1029/2004JC002784, 2005.

Stark, J. D., Donlon, C., O'Carroll, A., and Corlett, G.: Determination of AATSR biases using the OSTIA SST analysis system and a matchup database, J. Atmos. Ocean. Tech., 25, 1208–1217, 2008.

Stein, R. and MacDonald, R. W.: Organic carbon budget: Arctic ocean vs Global Ocean, in: The organic carbon cycle in the Arctic Ocean, Springer Verlag, Berlin, 315–322, 2004.

Stroeve, J., Serreze, M., Drobot, S., Gearheard, S., Holland, M., Maslanik, J., Meier, W., and Scambos, T.: Arctic sea ice extent plummets in 2007, Eos, 89, 13–14, 2008.

Takahashi, T., Sutherland, S. C., Wanninkhof, R., Sweeney, C., Feely, R. A., Chipman, D. W., Hales, B., Friederich, G., Chavez, F., Sabine, C., Watson, A., Bakker, D. C. E., Schuster, U., Metzl, N., Yoshikawa-Inoue, H., Ishii, M., Midorikawa, T., Nojiri, Y., Körtzinger, A., Steinhoff, T., Hoppema, M., Olafsson, J., Arnarson, T. S., Tilbrook, B., Johannessen, T., Olsen, A., Bellerby, R., Wong, C. S., Delille, B., Bates, N. R., and de Baar, H. J. W.: Climatological mean and decadal change in surface ocean $p\mathrm{CO}_2$, and net sea–air $CO_2$ flux over the global oceans, Deep-Sea Res. Pt II, 56, 554–577, doi:10.1016/j.dsr2.2008.12.009, 2009.

Tsai, W. and Liu, K. K.: An assessment of the effect of sea surface surfactant on global atmosphere-ocean $CO_2$ flux, J. Geophys. Res., 108, 3127, doi:10.1029/2000JC000740, 2003.

VLIZ: IHO Sea Areas: http://www.vliz.be/vmdcdata/vlimar/downloads.php, (last access: April), 2010.

Wang, M. and Overland, J. E.: A sea ice free summer Arctic within 30 years, Geophys. Res. Lett., 36, L07502, doi:10.1029/2009GL037820, 2009.

Wanninkhof, R.: Relationship between wind speed and gas exchange, J. Geophys. Res., 97, 7373–7382, 1992.

Weiss, R. F.: Carbon dioxide in water and seawater: the solubility of a non-ideal gas, Mar. Chem., 2, 203–215, 1974.

Weiss, R. F. and Price, B. A.: Nitrous oxide solubility in water and seawater, Mar. Chem., 8, 347–359, 1980.

Wolter, K.: Multivariate ENSO Index (MEI): http://www.esrl.noaa.gov/psd/enso/mei/, (last access:23 February 2012), 2012.

Wolter, K. and Timlin, M. S.: Measuring the strength of ENSO events: How does 1997/98 rank?, Weather, 53, 315–323, 1998.

Woolf, D. K.: Parameterization of gas transfer velocities and sea-state-dependent wave breaking, Tellus B, 57, 87–94, 2005.

Woolf, D. K., Leifer, I. S., Nightingale, P. D., Rhee, T. S., Bowyer, P., Caulliez, G., De Leeuw, G., Larsen, S. E., Liddicoat, M., and

Baker, J.: Modelling of bubble-mediated gas transfer: Fundamental principles and a laboratory test, J. Mar. Syst, 66, 71–91, 2007.
Zhang, T., Frauenfeld, O. W., Serreze, M. C., Etringer, A., Oelke, C., McCreight, J., Barry, R. G., Gilichinsky, D., Yang, D., and Ye, H.: Spatial and temporal variability in active layer thickness over the Russian Arctic drainage basin, J. Geophys. Res., 110, D16101, doi:10.1029/2004JD005642, 2005.
Žutić, V., Ćosović, B., Marcenko, E., Bihari, N., and Krsinic, F.: Surfactant production by marine phytoplankton, Mar. Chem., 10, 505–520, 1981.